https://doi.org/10.5194/hess-2022-241
Preprint. Discussion started: 18 July 2022
© Author(s) 2022. CC BY 4.0 License.

Hydrology and Earth System Sciences
Open Access
Discussions

Recent ground thermo-hydrological changes in a Tibetan endorheic catchment and implications for lake level changes

Léo C.P. Martin[1], Sebastian Westermann[2,3], Michele Magni[1], Fanny Brun[1,4], Joel Fiddes[5], Yanbin Lei[6,7], Philip Kraaijenbrink[1], Tamara Mathys[8], Moritz Langer[9,10], Simon Allen[11] and Walter W. Immerzeel[1]

1. Faculty of Geosciences, Utrecht University, Utrecht, The Netherlands
2. Department of Geosciences, University of Oslo, Blindern, 0316 Oslo, Norway
3. Center for Biogeochemistry in the Anthropocene, Oslo, Norway
4. Université Grenoble Alpes, CNRS, IRD, Grenoble INP, IGE, Grenoble, France
5. WSL Institute for Snow and Avalanche Research SLF, Davos, Switzerland
6. Key Laboratory of Tibetan Environment Changes and Land Surface Processes, Institute of Tibetan Plateau Research, Chinese Academy of Sciences, Beijing 100101, China
7. CAS Center for Excellence in Tibetan Plateau Earth System Sciences, Beijing 100101, China
8. Department of Geosciences, University of Fribourg, Fribourg, Switzerland
9. Alfred Wegener Institute Helmholtz Centre for Polar and Marine Research, 14473 Potsdam, Germany
10. Department of Geography, Humboldt Universität zu Berlin, 12489 Berlin, Germany
11. Department of Geography, University of Zurich, Zürich, Switzerland

Correspondence to: Léo Martin (leo.doug.martin@gmail.com)
Walter Immerzeel (w.w.immerzeel@uu.nl)

Abstract:	393 words
Main:	11,145 words, 10 figures, 1 table
Appendices:	515 words, 5 figures, 1 table

https://doi.org/10.5194/hess-2022-241
Preprint. Discussion started: 18 July 2022
© Author(s) 2022. CC BY 4.0 License.

Hydrology and Earth System Sciences
Discussions

Abstract

Climate change modifies the water and energy fluxes between the atmosphere and the surface in mountainous regions. This is particularly true over the Qinghai-Tibet Plateau (QTP), a major headwater region of the world, which has shown substantial hydrological changes over the last decades. Among them, the rapid lake level variations observed throughout the plateau remain puzzling and much is still to be understood regarding the spatial distribution of lake level trends (increase/decrease) and paces. The ground across the QTP hosts either permafrost or seasonally frozen ground and both are affected by climate change. In this environment, the ground thermal regime influences liquid water availability, evaporation and runoff. Therefore, climate-driven modifications of the ground thermal regime may contribute to lake level variations. For now, this hypothesis has been overlooked by modelers because of the scarcity of field data and the difficulty to account for the spatial variability of the climate and its influence on the ground thermo-hydrological regime in a numerical framework.

This study focuses on the cryo-hydrology of the catchment of Lake Paiku (Southern Tibet) for the 1980-2019 period. We use TopoSCALE and TopoSUB to downscale ERA5 data and capture the spatial variability of the climate in our forcing data. We use a distributed setup of the CryoGrid community model (version 1.0) to quantify thermo-hydrological changes in the ground during the period. Forcing data and simulation outputs are validated with weather station data, surface temperature logger data and the lake level variations. We show that both seasonal frozen ground and permafrost have warmed (1.7 °C per century 2 m deep), increasing the availability of liquid water in the ground and the duration of seasonal thaw. Both phenomena promote evaporation and runoff but ground warming drives a strong increase in subsurface runoff, so that the runoff/(evaporation + runoff) ratio increases over time. Summer evaporation is an important energy sink and we find active layer deepening only where evaporation is limited. The presence of permafrost is found to promote evaporation at the expense of runoff, consistent with recent studies. Yet, this relationship seems to be climate dependent and we show that a colder and wetter climate produces the opposite effect. This ambivalent influence of permafrost may help to understand the contrasting lake level variations observed between the south and north of the QTP, opening new perspectives for future investigations.

https://doi.org/10.5194/hess-2022-241
Preprint. Discussion started: 18 July 2022
© Author(s) 2022. CC BY 4.0 License.

Hydrology and Earth System Sciences Discussions

Main text

1. Introduction

Climate change is amplified in mountainous environments, with major consequences for ecosystems, landscapes, hydrology, human communities and infrastructure (IPCC, 2019). Station observations show that global warming is elevation dependent, the strongest warming rates being observed at high elevation (Pepin et al., 2015; Wang et al., 2014). Over the Qinghai-Tibet Plateau (QTP), a significant increase in surface air temperatures has been recorded since the 1980s (in particular in the North of the plateau, Zhang et al., 2022 and references therein). It is accompanied by a decrease in wind speed, a humidification of the air, and a general increase in precipitation, but with a strong spatial variability (Yang et al., 2014a). Altogether, these changes have affected the surface energy balance of the plateau through a shift of the Bowen ratio towards more latent heat fluxes, limiting the sensible surface warming (Bibi et al., 2018; Yang et al., 2014 and references therein).

These changes in water and energy fluxes between the atmosphere and the surface have the potential to alter the hydrological cycle of the QTP, which is the headwater region for major Asian rivers. As such, increasing trends of evaporation over land have been measured (3.8 mm per decade since the 1960s) with strong spatial variability both in absolute values and increase rates (Wang et al., 2020b). Changes in the seasonality of river discharge (Cao et al., 2006) and groundwater discharge (Niu et al., 2011) were reported for the same period. Overall glacier shrinkage is also observed since the 1960s with a persistent increase in glacier mass loss rates (Bhattacharya et al., 2021).

The QTP also features more than 1,000 lakes larger than 1 km^2 (Zhang et al., 2017), most of them located in endorheic catchments. Lake volume changes are therefore attributable to climatic and hydrological changes occurring within the lake catchment, such as glacier melt, ground ice melt, precipitation, evaporation or runoff patterns. A majority of these lakes have experienced a pronounced increase in water levels since the 1990s (Lei et al., 2013, 2014), a trend that was suggested to be mainly driven by changes in precipitation and evaporation patterns (Yao et al., 2018) rather than by an increase in glacier mass loss (Brun et al., 2020). Nevertheless, lake level variations are not uniform across the

https://doi.org/10.5194/hess-2022-241
Preprint. Discussion started: 18 July 2022
© Author(s) 2022. CC BY 4.0 License.

QTP and exhibit important spatial variability. Whereas the northern and central QTP have recorded lake expansion, the southern parts of the plateau have experienced lake shrinkage (Qiao et al., 2019; Zhang et al., 2020, 2021a). Such a complex pattern challenges our understanding of the hydrological changes occurring in these high Asian watersheds.

In this regard, new insights on hydroclimatic changes over the QTP can emerge from the investigation of the coupled energy and water fluxes between the ground surface/subsurface and the atmospheric boundary layer. These fluxes are driven by the climate and have a major impact on cold-region hydrology (Bring et al., 2016; Gao et al., 2021; Pomeroy et al., 2007). Indeed, hydrological variables (precipitation, evaporation, runoff) affect the soil water content, which changes its thermal properties, the distribution between latent and sensible fluxes and thus substantially influences the ground thermal regime (Bring et al., 2016; Koren et al., 1999; Martin et al., 2019). In turn, the ground thermal regime modifies the relative proportion of frozen and liquid subsurface water, influencing infiltration possibilities and the amount of water available for evaporation and surface/subsurface runoff (Carey and Woo, 2001; Yi et al., 2006). So far, climate induced thermo-hydrological changes over the QTP have received limited attention. Large-scale modeling studies reported changes in the seasonal ground freezing cycles characterized by a reduction of the frost depth and duration of the frozen period since the 1960s (Qin et al., 2018; Wang et al., 2020a) and notable ground warming trends in summer and winter (Qin et al., 2021). Additionally, ground warming over the QTP was reported to promote evaporation and to decrease runoff (Qin et al., 2017; Wang et al., 2020b).

Complementary to seasonally frozen ground, permafrost is also a distinctive feature of climate-surface interactions in cold regions. Large-scale permafrost modeling suggests that it covers a significant part of the QTP, mainly as continuous permafrost in the north of the plateau and as discontinuous or sporadic in the south (Obu et al., 2019). Permafrost on the QTP has usually a low ice content due to limited precipitation and strong evaporation (Wu et al., 2005; Yang et al., 2010). Borehole temperature measurements show that it is a relatively warm type of permafrost (Biskaborn et al., 2019; Wu and Zhang, 2008) and its exposure to high solar radiations makes it sensitive to changes in surface conditions and climate change (Yang et al., 2010). Since the 1960s, climate change has driven the warming of permafrost across the plateau (Ran et al., 2018; Shaoling et al., 2000). Ran et al. (2018)

reports that most of the plateau exhibit a warming trend of the ground comprised between 2.6 and 7.4 °C per century and half of the plateau warms at a rate higher than 5 °C per century. This warming is accompanied by upward migration (of around 100 m between the 1960s and 2000s) and shrinkage of permafrost covered areas (24% of permafrost extent lost between the 1960s and 2000s, Ran et al., 2018).

Permafrost grounds are characterized by a strong interplay between the ground thermal regime and the land hydrology. Seasonal thawing and freezing of the active layer is driven by the surface energy balance and in return, influences surface and subsurface runoff (Kurylyk et al., 2014; Sjöberg et al., 2021; Walvoord and Kurylyk, 2016) and evaporation (Gao et al., 2021). In this regard, both large scale and regional modeling indicates that thawing permafrost enhances evapotranspiration (Qin et al., 2017; Wang et al., 2020b). Qin et al. (2017) also reports that the increase in evaporation is logically concomitant with a decrease in runoff. Additionally, permafrost stores water as ground ice and its thawing can trigger the release of liquid water in the watershed, contributing up to 15% of the yearly river streamflow (Cheng and Jin, 2013; Yang et al., 2019).

The aforementioned hydrological changes are tied to various interdependent climate-driven physical processes happening at the ground surface and subsurface (e.g. surface energy balance, infiltration, water phase change, heat conduction...). Because these processes exhibit a strong spatial variability in high mountain environments, they are challenging to represent accurately together on large spatial scales. Therefore, a deeper understanding of the impact of ground thermo-hydrological changes on the High Asia water cycle can be gained through small-scale physical modeling of these processes. Yet, for now, physics-based approaches at the catchment scale aiming to connect the ground thermo-hydrological regime and the observed hydrological changes on the QTP (such as lake level changes) remain scarce. They are however a powerful approach to tackle the question: how much climate-driven ground thermal changes might affect the water cycle in high mountain headwater regions? In this study, we use physical land surface modeling to quantify the ground thermo-hydrological changes of an endorheic Tibetan catchment over the last 40 years as a response to climate change. We show the interplay in the water and energy fluxes occurring between the atmosphere, the surface and the subsurface and discuss their impact on the hydrology of the catchment and their implication regarding lake level variations.

https://doi.org/10.5194/hess-2022-241
Preprint. Discussion started: 18 July 2022
© Author(s) 2022. CC BY 4.0 License.

Hydrology and Earth System Sciences
Discussions

2. Study area: the Paiku catchment

The Paiku catchment is located in south-western Tibet, China, close to the border with Nepal (28.8°N - 85.6°E, Fig. 1). Its southern edge lies 7 km from the Shishapangma peak (8027 masl). The catchment is endorheic and spans over 78 km from North to South, 66 km from East to West and covers 2 400 km^2. The median elevation of the catchment is 4872 masl, ranging from 7272 masl to its lowest point, the lake Paiku at 4580 masl. Geologically, the catchment is mainly located in the Tethys Himalayan, and thus, an important part of the formations underlying the catchment are metamorphized sedimentary series. The southern part of the catchment crosses the Southern Tibetan Detachment, and thus, the southern ridges of the massif belong to the High Himalayan metamorphic formations in the west and to the High Himalayan leucogranites of the Shishapangma massif on the east. The north and north-east ridges are formed by granite intrusions surrounded by metamorphic domes. The inner part of the catchment presents Plio-Quaternary formations such as alluvial fans close to the ridges and inclined alluvial plains in its inner parts (Fig. B of the appendices, Aoya et al., 2005; Searle et al., 1997; Wünnemann et al., 2015).

Automatic Weather Station (AWS) observations (5033 masl, Oct 2019 – Sept 2021, Fig. 1) show that the climate in the catchment is characterized by a relatively small temperature amplitude during the year (around 20 °C, JJA being the warmest months and DJF the coldest) and significant daily amplitude (up to 10 °C during the warm season). The mean annual temperature is -1.5 °C at the AWS, where night freezing can occur until the beginning of June and restart at the beginning of October. The catchment is dry (~ 200 mm $year^{-1}$) and precipitation mostly fall as rain during the monsoon (JJAS).

Around 5% of the catchment is covered by glaciers (RGI Consortium, 2017), which are concentrated in its southwestern part. They feed several proglacial lakes that can reach up to 6 km in length. Geodetic glacier mass budgets show that, similar to other glaciers in the region, glaciers of the Paiku catchment have undergone sustained mass loss at least since the 1970s, with an average mass balance of -0.3 m $w.e.a^{-1}$ until the beginning of the 2000s and around -0.4 m $w.e.a^{-1}$ afterwards (Bhattacharya et al., 2021). There are more than 10 rivers that drain the catchment towards the lake and most of them only exhibit a seasonal activity during the monsoon months. The three main ones are (Fig.

https://doi.org/10.5194/hess-2022-241
Preprint. Discussion started: 18 July 2022
© Author(s) 2022. CC BY 4.0 License.

Hydrology and Earth System Sciences
Discussions

1), Daqu (glacier-fed, 450 km^2), Bulaqu (glacier-fed, 325 km^2) and Barixiongqu (non-glacier-fed, 703 km^2) (Lei et al., 2018).

In the north-west of the catchment, Lake Paiku covers approx. 280 km^2 (11.5% of the catchment surface area) and spans over 27 km from north to south. It has a mean water depth of 41 m, with a maximum water depth of 73 m (Lei et al., 2018). It receives water from direct precipitation and from land and glacier runoff which can be routed at the surface via the river systems or the subsurface via the alluvial formations. Because it is hydrologically closed, the lake mainly loses water through evaporation. Previous studies reported lake level fluctuations over different time scales. It reached 4665 masl (85 m higher than present level) prior to 25 ka BP and at the onset of the Holocene (11.9-9.5 ka BP). Afterwards, the lake shrank gradually (Wünnemann et al., 2015). More recently, the lake level decreased by 3.7 m between 1972 and 2015, losing 4.2% of its surface and 8.5% of its volume (Fig. 2, Lei et al., 2018). At the seasonal scale, the lake level cycle has an amplitude of ~ 0.4 m. It is marked by a strong increase during the monsoon period (JJAS) supported by direct precipitation, glacier melt and land runoff. From October and until the next monsoon period, evaporation dominates the lake mass budget and the level decreases rapidly until January and at a slower rate afterwards (Lei et al., 2021).

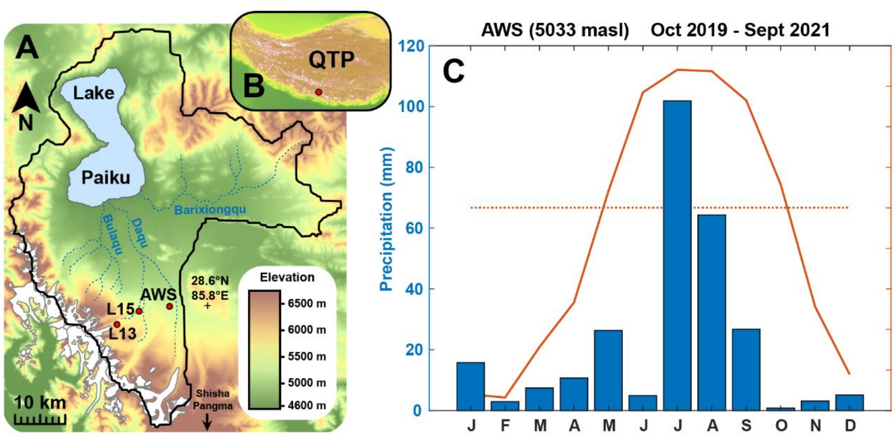

Figure 1. The Paiku Catchment. A: Topographic and hydrologic map of the catchment with the glaciers in white, the ephemeral rivers in dark blue and the lake in light blue. AWS: Automatic Weather Station. L13 and L15 are surface temperature loggers (Sect. 3.1). B: Localization of the catchment over the QTP. C: Monthly temperature and precipitation recorded at the AWS between October 2019 and September 2021.

https://doi.org/10.5194/hess-2022-241
Preprint. Discussion started: 18 July 2022
© Author(s) 2022. CC BY 4.0 License.

3. Material and methods

3.1. Field measurements

An AWS was set up in October 2019 in the South of the catchment at an elevation of 5033 masl (Fig. 1). It is equipped with various sensors which record air temperature, pressure, relative humidity, wind speed, incoming and outgoing long and short wave radiations and precipitation every 15 minutes. The meteorological record extends to September 2021 and covers a period of nearly 2 years. We used it to evaluate and correct the distributed downscaled climatic forcing we used in our modeling framework (Sect. 3.2.5.).

Two temperature loggers recorded the surface temperature in the vicinity of the AWS location. Logger 15 (L15) is located at 5055 masl, 6 km west from the AWS. Logger 13 (L13) is located at 5356 masl, 12 km west from the AWS (Fig. 1). Both loggers were buried 10 to 15 cm below the surface to avoid direct solar radiation on the sensors and recorded surface temperature at a 20 minutes time step from October 2017 to October 2018. These surface temperature records were used to evaluate the simulations (Sect. 3.2.5.).

3.2. Catchment thermo-hydrological modeling

3.2.1. Conceptual hydrological model for the catchment

In order to understand the level variations of lake Paiku over the last 40 years (1980-2019 period), we develop an approach at the catchment scale. Because the catchment is hydrologically closed, the lake receives water input via direct precipitation, land surface and subsurface runoff and glacier runoff. Conversely, it only loses mass via evaporation. As such, the present study requires quantification of all these terms of the hydrological balance. The production of forcing data for the catchment (including precipitation) is detailed in Sect. 3.2.2. The land hydrology processes are quantified using the CryoGrid community model (version 1.0) (Westermann et al., 2022) as described in section 3.2.3. Distributed 1D simulations are used to quantify land evaporation and runoff. The routing of water in the catchment is not represented and the runoff computed for a given simulation is directly accounted as a water input for the lake. The evaporation from the lake is simulated using the CryoGrid3-Flake model (Langer et

https://doi.org/10.5194/hess-2022-241
Preprint. Discussion started: 18 July 2022
© Author(s) 2022. CC BY 4.0 License.

al., 2016) as described in Section 3.2.4. Glacier melt is not modeled, but estimated for the study period (1980-2019) from remote sensing observations. From these observations, glaciers yield is calculated as described in Sect. 3.2.6. Our catchment-scale approach to represent the hydrological balance of the lake is summarized in Fig. 2.

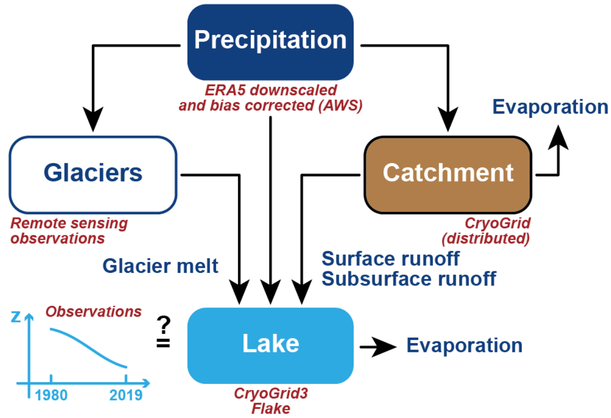

Figure 2. Conceptual hydrological framework for the study.

3.2.2. Forcing data production and validation

In high mountain environments, topography creates strong spatial variability of temperature and incoming radiation, which impact the surface energy balance (Klok and Oerlemans, 2002) and the ground thermo-hydrological regime (Magnin et al., 2017). Our approach requires forcing data that (i) captures this variability, (ii) includes numerous variables such as air temperature, incoming long and short wave radiations, wind speed, specific humidity, rain and snowfall and (iii) cover the 40 years study period at a sub-daily timestep. The TopoSCALE approach (Fiddes and Gruber, 2014) was developed for this purpose and allows to downscale reanalysis products like ERA5 (Hersbach et al., 2020) at high resolution (here ~ 100 x 100 m). Additionally, because working at a 10^{-2} km^2 spatial resolution over a 2400 km^2 catchment would require more than 200,000 forcing files and simulations, we rely on the TopoSUB method (Fiddes and Gruber, 2012) to reduce computational costs. This method uses a SRTM30 Digital Elevation Model to explore redundancies in physiographic parameters of the study area such as elevation, aspect, slope and sky-view factor and identify groups of high resolution pixels (100 x 100 m) sharing similar values for these parameters. From there, all the high resolution pixels belonging to such a group are only described as a single TopoSUB point for which climatic

https://doi.org/10.5194/hess-2022-241
Preprint. Discussion started: 18 July 2022
© Author(s) 2022. CC BY 4.0 License.

Hydrology and Earth System Sciences
Open Access
Discussions

variables can be downscaled to create one single dataset of climatic timeseries. The degree of similarity required by TopoSUB to identify groups of high resolution pixels with redundant physiographic parameters can be adjusted by choosing the final number of TopoSUB points (and thus climate datasets) that should be used to cover the area corresponding to one ERA5 pixel. The Paiku catchment intersects 8 ERA5 pixels at 30 km resolution and we chose to use 50 TopoSUB points within each ERA5 pixels to cover the spatial variability created by the topography on small-scale climate. Ultimately, 368 TopoSUB points are used to cover the catchment. The average level of redundancy (i.e. the average number of high resolution pixels represented by a single TopoSUB point) is 723 ± 745 (1σ, median: 506, min: 1, max: 4347). Fig. C shows the distribution of the TopoSUB points and a reconstruction of the topography of the catchment based on this approach. The period covered by the forcing datasets starts on 1st January 1980 and ends on 31st August 2020 (40 years and 8 months).

In the TopoSCALE statistical downscaling approach, we do not rely on the AWS data and thus the downscaled ERA5 data can be biased, as is often the case over Asia (Jiang et al., 2020, 2021; Jiao et al., 2021; Orsolini et al., 2019). Comparison against the available AWS observations (Fig. D) indeed highlights notable differences in variables such as air temperature and precipitation. From these differences we derived monthly bias correction factors that we apply systematically to all of the 368 climate forcing datasets. The catchment-averages for precipitation and air temperatures are shown in Fig. 3.

https://doi.org/10.5194/hess-2022-241
Preprint. Discussion started: 18 July 2022
© Author(s) 2022. CC BY 4.0 License.

Hydrology and Earth System Sciences
Discussions
Open Access

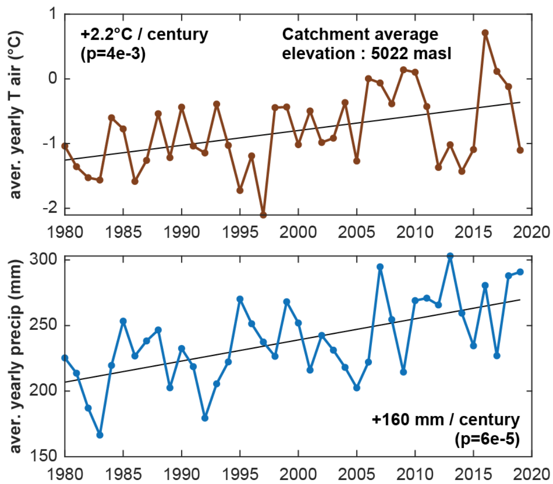

Figure 3. Climate forcing data for the land and lake modeling. Yearly catchment-average air temperature (2 m above ground) and total precipitation for the study period. Note that the model is also forced by incoming short and long wave radiations, humidity, windspeed and air pressure. Details about the spatial and temporal resolution of the distributed forcing data are presented in in Sect. 3.2.2.

3.2.3. The CryoGrid community model (version 1.0)

To simulate the ground thermo-hydrological regime, we use the CryoGrid community model (Westermann et al., 2022). The CryoGrid community model (CG) is a land surface model designed for applications in cold regions where seasonal frozen ground or permafrost may occur. The model implements heat transfer in a 1D soil column, accounting for freeze-thaw processes of soil water using effective heat capacity (Nakano and Brown, 1972). To do so, soil freezing curves are based on Dall'Amico et al. (2011) as detailed in Westermann et al. (2013). Vertical water movement in the soil column is based on Richards equation (Richards, 1931; Richardson, 1922). The soil matric potential and hydraulic conductivity follow van Genuchten (1980) and Mualem (1976). The model features the snowpack module called *CG Crocus* described in Zweigel et al. (2021) that adapts the snow physics parameterizations from the CROCUS scheme (Vionnet et al., 2012) to the native snow module of CryoGrid3 (Westermann et al., 2016). At the surface, the model uses a surface energy balance module to calculate the ground surface temperature and water content. The turbulent fluxes of sensible and latent heat are calculated using a Monin–Obukhov approach (Monin and Obukhov, 1954). Evaporation is adjusted to the available water in the soil and the water loss is distributed vertically to decreases exponentially with depth.

https://doi.org/10.5194/hess-2022-241
Preprint. Discussion started: 18 July 2022
© Author(s) 2022. CC BY 4.0 License.

3.2.4. Model setup and validation

The setup of the CryoGrid community model for land is presented in Fig. 4. To capture the high spatial variability of mountainous climate, our approach relies on the 368 climate forcing datasets to cover the catchment (see section 3.2.3). This approach enables us to perform spatially distributed modeling. All of the 368 simulations are independent and use the same parameterization. In absence of direct observation of the soil stratigraphy within the catchment, the soil column was designed to agree with field observations in the region (Hu et al., 2020; Luo et al., 2020; Wang et al., 2008, 2009; Yang et al., 2014b; Yuan et al., 2020), to be consistent with similar modeling approaches across Tibet (Chen et al., 2018; Song et al., 2020) and to be consistent with input datasets (Shangguan et al., 2013, 2017). Thus, the soil stratigraphy is divided in 3 units: a top soil (0.3 m thick), a bottom soil (1.7 m thick) and a bedrock unit (extending beyond the depth of interest of the study). An overview of the parameters for each unit, their source and the way they are calculated is presented in Table A. Regarding the processes implemented in the model (Sect. 3.2.3), infiltration according to Richards equation only occurs in the top and bottom soil units. The bedrock unit has a static water content. Additionally, to simulate subsurface runoff towards the lake, the two soil units are hydrologically connected to a reservoir at the elevation of the lake. This reservoir drains excess water of the soil column when its water content exceeds field capacity. This drainage is quantified using Darcy's law and relies on a hydraulic slope taken as the mean slope of the catchment.

Because we do not have knowledge of the distributed thermal state with depth over the catchment at the beginning of the simulations, we assume temperature profiles were in equilibrium with the climate of the 5 first years of modeling (1980-1984). To do so, we start our simulations with a 60 years spin-up of these first 5 years (12 repetitions), which is sufficient to establish a stable temperature profile in the hydrologically active part of the ground (the first 2 meters).

https://doi.org/10.5194/hess-2022-241
Preprint. Discussion started: 18 July 2022
© Author(s) 2022. CC BY 4.0 License.

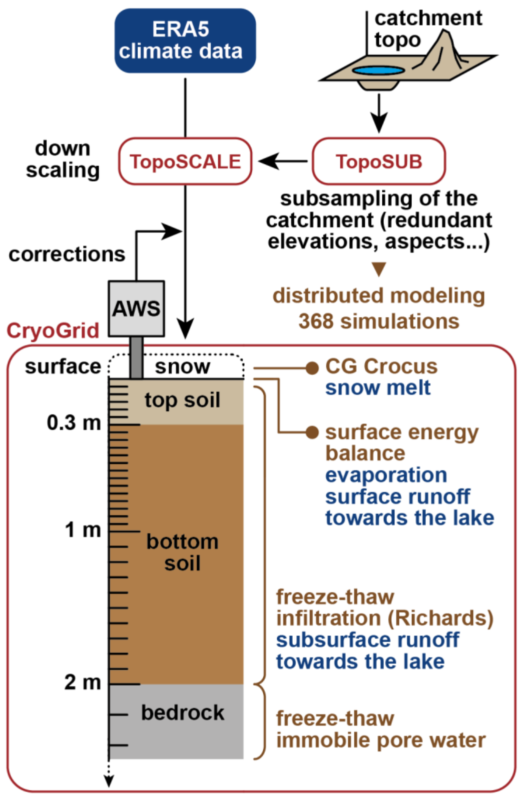

Figure 4. Modeling framework for the land hydrology. ERA5 data are downscaled using the TopoSUB and TopoSCALE approaches (Fiddes and Gruber, 2012, 2014). The downscaled data are bias-corrected based on the AWS observations. Distributed 1D simulations are performed using the CryoGrid community model (Westermann et al., 2022). The vertical resolution is indicated with the tick marks on the depth axis.

To validate model simulations, the simulated ground surface temperatures (GST) are compared to the two temperature logger time series acquired in the vicinity of the AWS (Sect. 3.1). We used this comparison to calibrate the surface roughness used for the surface energy balance calculations in the model.

3.2.5. Lake modeling

The lake thermo-hydrological response to the climatic forcing data is simulated using the CryoGrid3-Flake model (Langer et al., 2016). The two models were coupled by Langer et al. (2016) to simulate the thermal regime of thermokarst lakes (including surficial water freezing and melting) and underlying ground. Here we use the coupled models mainly to quantify evaporation at the lake surface. In the coupled model, the native surface energy balance module of CryoGrid3 (Westermann et al., 2016)

https://doi.org/10.5194/hess-2022-241
Preprint. Discussion started: 18 July 2022
© Author(s) 2022. CC BY 4.0 License.

was amended to account for processes tied to free water surface energy balance: (i) the dependance of the albedo of a water surface to solar angle (and thus time of the day) and wind speed (and wave formation), (ii) the dependance of the surface roughness length to wind speed (and wave formation) and (iii) the exponential decay of incoming radiation with depth in the water column. Similarly to the land simulations, the lake simulations were forced by the downscaled ERA5 data, with the corrections derived from the AWS data (Sect. 3.2.2). The simulations were initiated with a 20 years spin-up of the 1980-1984 climate.

3.2.6. Quantification of glacier mass change

Multiple studies quantified the volume change of the glaciers located within Paiku catchment in the recent past (1970s to 2020). There are no field based measurements of glacier mass balance available in this catchment to our knowledge. As a consequence, we rely solely on the geodetic mass balance studies (Brun et al., 2017; Hugonnet et al., 2021; King et al., 2019; Maurer et al., 2019; Shean et al., 2020). All these studies estimated glacier volume changes over periods of 20-30 years from satellite derived DEMs. As a consequence, we can only estimate the average annual glacier mass balance, and not the year to year variability. Glaciers occupy approximately 113 km^2 in the Paiku catchment. They have shrunk for the past fifty years at a rate of 0.44 % y^{-1}, from an area of 132 km^2 in 1975 to 122 km^2 around 2000 and to their current extent (Bolch et al., 2019; King et al., 2019). The average mass balances for the period 1975-2000 and 2000-2020 are $-3.9 \pm 2.1\times10^{10}$ kg y^{-1} and $-5.4 \pm 2.4\times10^{10}$ kg y^{-1}, respectively ($-4.6 \pm 2.5\ 10^7$ m^3 and $-6.4 \pm 2.8\ 10^7$ m^3 with a 850 kg m^{-3} density). These mass balances correspond to specific mass balances of -0.31 ± 0.17 m of water equivalent per year (w.e. y^{-1}) and -0.47 ± 0.21 m w.e. y^{-1}, respectively.

https://doi.org/10.5194/hess-2022-241
Preprint. Discussion started: 18 July 2022
© Author(s) 2022. CC BY 4.0 License.

4. Results

4.1. Model validation and lake evaporation

Model validation results are presented in Fig. 5. Simulated daily ground surface temperatures are in good agreement with the observed ones with a bias of -0.2 °C and 0.6 °C and a RMSE of 1.4 °C and 1.6 °C for loggers 15 and 13 respectively (Fig. 5A and 5B). Most of this RMSE is explained by a mismatch between model and observations in the tails of the temperature distribution, whereas intermediate temperatures exhibit the best agreement with observations.

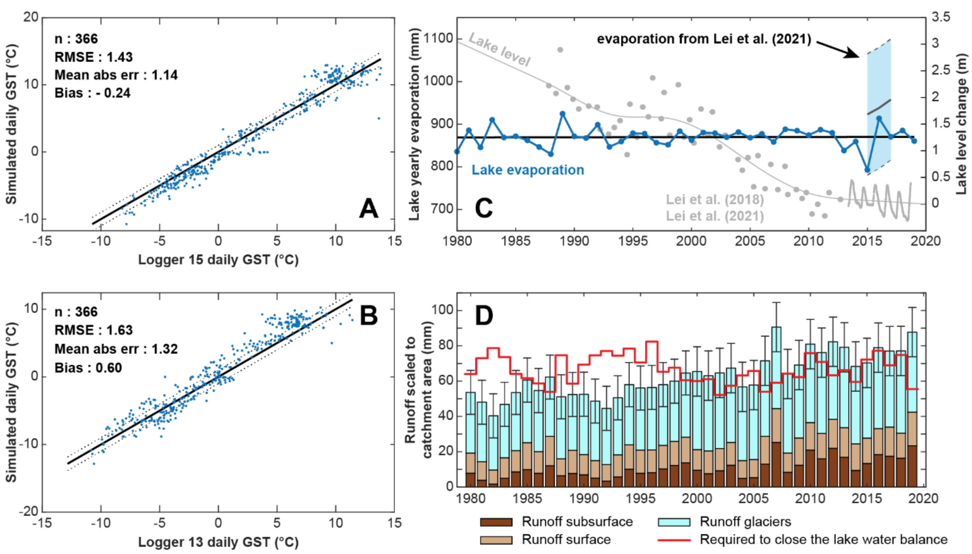

Figure 5. Model validation. A and B: modeled mean daily ground surface temperatures compared to measured ground surface temperatures for logger 15 and logger 13 (location on Fig. 1). C: modeled yearly lake evaporation (blue curve) and comparison with values calculated by Lei et al. (2021) in the light blue zone. The grey curve shows the smoothed lake level variations based on observations from Lei et al. (2018) (grey points) and Lei et al. (2021) (grey oscillating line). D: Comparison between the runoffs required to reproduce the observed lake variations (red curve, derived from lake level, lake area, forcing data and lake evaporation) and the sum of the glacier and land runoff we derive from remote sensing observations and modeling respectively (Sect. 3.2). Error bars are associated to the glacier values and come from the geodetic results. Runoff values are expressed as heights scaled to the land surface of the Paiku catchment.

Yearly lake evaporation mainly ranges between 800 and 900 mm per year, with a mean value of 870 ± 23 mm (1σ). Lake evaporation does not exhibit a linear trend of increase or decrease and is mostly dominated by year to year variability. Though slightly lower, our evaporation results are in agreement with the values from Lei et al. (2021), which are derived from local and regional meteorological observation and lake budget calculation (Fig. 5, C). We used the simulated evaporation together with the lake level data and lake area data from Lei et al. (2018) and Lei et al. (2021) and the precipitation forcing datasets (3.2.2) to derive the total runoff (land + glacier) required as an input to the lake budget to reproduce the lake variations. This required runoff corresponds to the red line of Fig. 5D. The required runoff volumes are scaled to the land area of the catchment to be comparable with the other variables. The fact that these values are substantially higher than 0 mm per year highlights the importance of the land and glacier contribution to the lake budget.

Fig. 5D also presents the runoff values derived from the land cryo-hydrological modeling and from the glacier remote sensing investigations. Annual volumes are expressed as mm over the land part of the catchment (excluding the lake). Based on the characteristics of remotely sensed observations, glacier mass balance values are considered constant for the 1980-2000 period and 2000-2019 period and respectively equal to $-4.6 \pm 2.5\ 10^7$ and $-6.4 \pm 2.8\ 10^7\ m^3$ per year. The addition of yearly precipitation to these values to quantify the total glacier runoff introduces year to year variability to the glacier runoff. At the catchment scale, the average glacier runoff over the 40 years is 39 ± 13 mm per year.

Over the 40 years, the average yearly land runoff value (surface + subsurface) we model is 24 ± 8 mm. Summed together, the land and glacier runoff find a partial agreement with the runoff that is required to close the lake water balance. Yearly values are compatible within error bars for 28 out of the 40 years of simulations. The glacier and land runoff are slightly too small to close the lake water balance during the first 20 years, and slightly too large for the last 20 years of simulation. Over the whole period, the sum of the glaciers + land runoff produces 95% of the required runoff. Land runoff is further described in Sect. 4.3.

https://doi.org/10.5194/hess-2022-241
Preprint. Discussion started: 18 July 2022
© Author(s) 2022. CC BY 4.0 License.

Hydrology and Earth System Sciences
Discussions

4.2. Ground thermal results

Thermal results are summarized in Fig. 6, Tab. 1 and the Fig. 7. The maps A and B of Fig. 6 show the active layer thicknesses throughout the catchment, averaged for the 1980-1989 and 2010-2019 periods. If there is an active layer present in map A but not in map B, the permafrost disappeared during the simulation (represented in grey in Fig. 6B). From 1980 to 1989, permafrost covers 27% of the catchment and the mean active layer thickness is 1.36 ± 0.51 m (1σ, minimum: 0.11 m and maximum: 2.37 m). From 2010 to 2019, permafrost covers 22% of the catchment. At the scale of the initial permafrost area, this change corresponds to a loss of 19%. The mean active layer thickness is 1.29 ± 0.49 m (1σ, minimum: 0.11 m and maximum: 2.55 m) for this period. Permafrost disappearance mainly happens for low-lying permafrost of the south and the center of the catchment. It occurs for the most part on the outer slopes of the permafrost regions and at the bottom of steep glacial valleys.

Maps C and D present 8 m depth temperatures fields for the months of December, January and February averaged for the same two decades. While the mean temperature for the first decade of the simulation is 1.83 °C, it is 2.37 °C for the last decade. This deep warming is associated with a migration of the 0 °C isotherm from 5260 masl to 5320 masl (+60 m). The warming trend is not spatially uniform and varies with elevation. The mean ΔT_{8m} (difference between the 2010-2019 and the 1980-1989 period) is the strongest at the bottom of the catchment where it reaches +0.68 ± 0.23 °C for the 4500-5000 masl elevation range and decreases linearly with elevation until +0.09 ± 0.14 °C beyond 6000 masl.

https://doi.org/10.5194/hess-2022-241
Preprint. Discussion started: 18 July 2022
© Author(s) 2022. CC BY 4.0 License.
Hydrology and Earth System Sciences
Open Access
Discussions

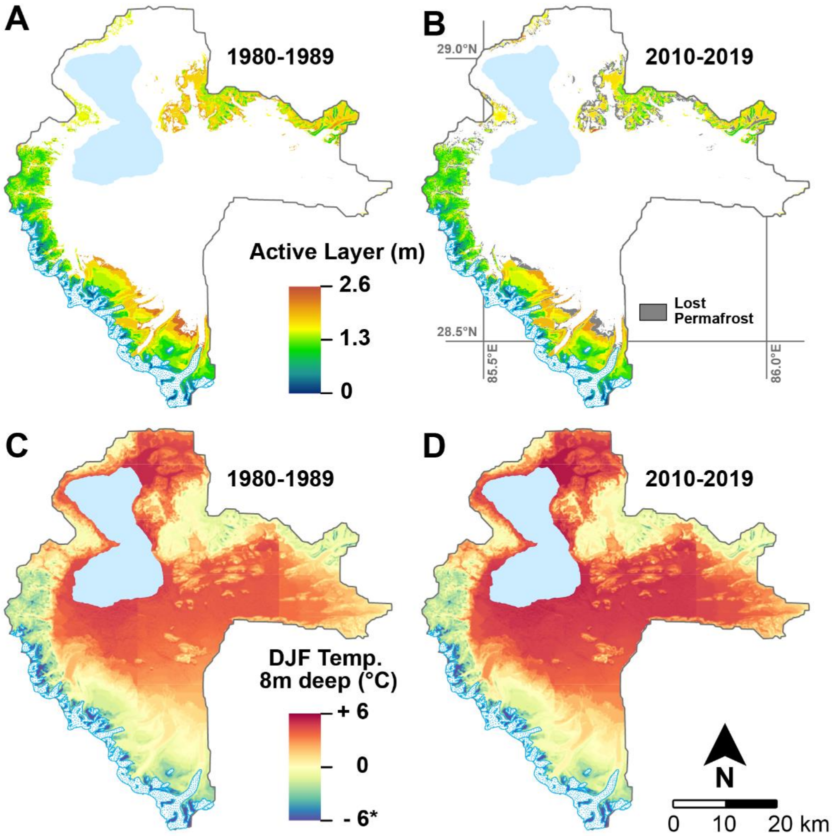

Figure 6. Thermal result maps. A: Average active layer depth over the 1980-1989 period. B: Average active layer depth over the 2010-2019 period. Only locations presenting permafrost at the end of the simulation are assigned a color on the map. Locations which underwent permafrost disappearance appear in grey on B. C: Average 8m-deep ground temperature for December, January and February for the 1980-1989 period. D: Average 8m-deep ground temperature for December, January and February for the 2010-2019 period.

Based on the active layer results, we define four categories of ground thermal regimes. *Cold permafrost* are the areas of the catchment for which the deepest thaw depth did not exceed 1 m over the 40 years of simulation. For cold permafrost, frozen conditions dominate the first meters of the ground most of the year and surficial thawing during summer is limited and does not give rise to a distinct active layer season. *Warm permafrost* are the areas of the catchment presenting permafrost for the whole duration of the simulation and which are not part of the *cold permafrost*. These areas are characterized by a distinct seasonal pattern of frozen ground in winter and active layer in summer. *Disappearing permafrost* are the areas of the catchment presenting permafrost at the beginning of the simulation and

https://doi.org/10.5194/hess-2022-241
Preprint. Discussion started: 18 July 2022
© Author(s) 2022. CC BY 4.0 License.
Hydrology and Earth System Sciences
Discussions

not at the end. *No permafrost* are the areas without permafrost at the onset of the simulation. The geographical characteristics of each ground category is presented in Tab. 1, their distribution throughout the catchment is shown on Fig. F of the appendices. These different ground categories are subsequently used to compare their cryo-hydrological behaviors during the simulation (consistent color code).

Table 1. Cryological classification of the catchment based on the modeled ground temperatures

Name	Characteristics	% of the catchment area	Elevation mean (masl)	Elevation range (masl)	Slope mean (°)
Cold permafrost	Max thaw depth over the 40 years < 1m	3%	6068	6946 5213	35±13
Warm Permafrost	Max thaw depth > 1 m and permafrost present over the 40 years	19%	5480	5921 4877	20±9
Disappearing permafrost	Permafrost present in 1980 but disappears during the simulation	5%	5274	5552 4882	18±9
No permafrost	No permafrost from 1980 to 2019	73%	4900	5463 4580	10±8

Fig. 7A shows the yearly temperature at a 2 m depth averaged for the whole catchment and for each cryological state of the ground. At the catchment scale, the 2 m depth temperature shows a pronounced warming trend of 1.7 °C per century ($p=1\times10^{-6}$). This trend is mainly supported by the *no permafrost* areas, which underwent a slightly stronger warming trend of 2.0 °C per century ($p=7\times10^{-8}$). Areas with disappearing permafrost, warm permafrost and cold permafrost exhibit smaller trends around 1 °C per century with decreasing p-values (respectively 0.00001, 0.006 and 0.05).

Fig. 7B shows the average duration of seasonal thawing at a depth of 70 cm averaged over the catchment. Because at this depth some areas might present two (or more) consecutive years without thawing (highest locations) or without freezing (lowest locations), these areas were excluded from the averaging. In the end, the averaged results account for 89% of the catchment land area (i.e. excluding glaciers and lake). The results show an increasing trend in the duration of the seasonal thaw of +46 days per century ($p=3\times10^{-4}$). When looking at the average start and stop days of the seasonal thaw in the Julian calendar (day 150 is the 30th of May and day 300 is the 27th of October), we note that this increase is mainly caused by a later ending date of the thaw season (*Stop date* on Fig. 7, +61 days per century, $p=8\times10^{-10}$) and not by an earlier starting date (+14 days per century, p=0.09).

https://doi.org/10.5194/hess-2022-241
Preprint. Discussion started: 18 July 2022
© Author(s) 2022. CC BY 4.0 License.

Hydrology and Earth System Sciences
Open Access
Discussions

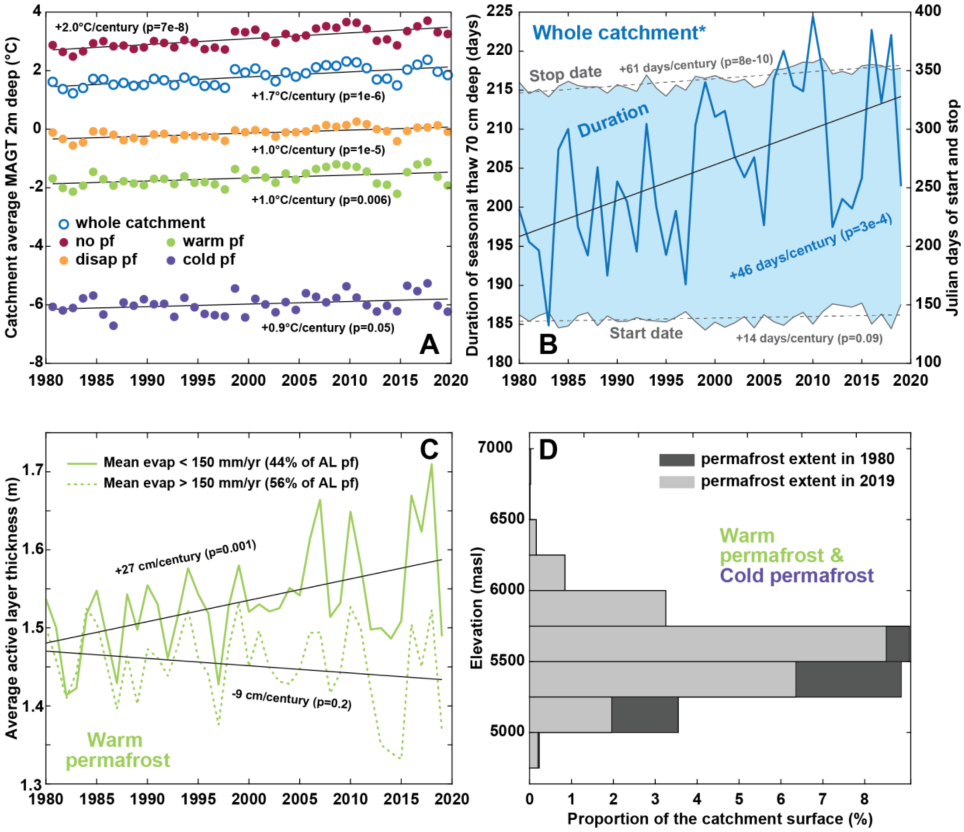

Figure 7. Ground thermal results. A: Yearly 2 m deep ground temperature averaged for the whole catchment and for the different cryological states of the ground (see Tab. 1). B: duration of seasonal thaw 70cm deep averaged over the catchment. The asterisk indicates that the presented curves average 89% of the surface of the catchment (Sect. 4.2). The grey curves and the light blue area are associated with the right axis and indicate the average start and stop day of the seasonal thaw in the Julian calendar. Values higher than 365 indicates that freezing conditions came back after the 31st of December. C: active layer thickness (ALT) evolution for warm permafrost. The solid line shows the ALT for simulations experiencing a yearly evaporation lower than 150 mm when averaged over the 40 years. The dashed line shows the ALT for simulations with yearly evaporation higher than 150 mm. D: Altitudinal distribution of permafrost in 1980 and 2019. This distribution includes both cold and warm permafrost.

Fig. 7C shows active layer thickness trends for *warm permafrost*. Within *warm permafrost*, AL thickness is presented for locations experiencing an average evaporation lower or higher than 150 mm per year during the simulations. Whereas location with average evaporation below 150 mm per year record an active layer deepening trend of 27 cm per century (p=0.001), it is not the case for locations with an average evaporation higher than 150 mm per year (p=0.2, non-significative trend).

https://doi.org/10.5194/hess-2022-241
Preprint. Discussion started: 18 July 2022
© Author(s) 2022. CC BY 4.0 License.

Fig. 7D compares permafrost spatial distribution between 1980 and 2019. These results show that permafrost distribution above 5750 masl has not been modified during the simulation. Permafrost disappearance has mainly occurred between 5000 and 5750 masl, with the largest loss reaching 2.5% of the catchment area between 5250 and 5500 masl.

In the permafrost-free areas of the catchment, seasonal frozen ground reaches a depth of 1.43+0.15 m on average and shows a decreasing trend of -68 cm per century ($p=6\times10^{-4}$, Fig. E). At a 70 cm depth, the average duration of seasonal frozen ground is 136 ± 12 days with a decreasing trend of -53 days per century ($p=4\times10^{-4}$). These values average 88% of the no permafrost areas since locations showing persistent thawed conditions from one year to another were excluded.

4.3. Hydrological results

Hydrological results are summarized on Fig. 8. Fig. 8A shows the yearly evaporation averaged over the whole catchment (land area only). The mean yearly evaporation over the simulation time is 180 ± 19 mm (1σ). Evaporation shows an increasing trend over the 40 years of +101 mm per century ($p=3\times10^{-7}$). Average total runoff over the 40 years is 24±8 mm per year and exhibits an increasing trend of +48 mm per century ($p=8\times10^{-7}$). Similarly, surface runoff (13 ± 3 mm per year) and subsurface runoff (11 ± 6 mm per year) show increasing trends of +13 and +35 mm per century ($p=6\times10^{-5}$ and 3×10^{-7}) respectively. The surface runoff presented on Fig. 8 includes the snow melt that did not infiltrate the ground.

Fig. 8C presents the catchment average of the *runoff / (runoff + evaporation)* ratio, which is equivalent to *runoff / (rain + snow – snow sublimation)* given the negligeable contribution of soil storage variations. Hence it is the proportion of the water input to the ground surface that is converted into runoff. This proportion is 11 ± 2% over the simulation time and shows an increasing trend of +13% per century ($p=2\times10^{-7}$). The graph also shows the average theoretical ratio to maintain a steady lake level of 17.6%. This ratio was obtained under the following hypothesis:

https://doi.org/10.5194/hess-2022-241
Preprint. Discussion started: 18 July 2022
© Author(s) 2022. CC BY 4.0 License.
Hydrology and Earth System Sciences
Open Access
Discussions

- Same climate forcing data, hence same lake evaporation
- The glacier contribution is (i) considered the same for the historical simulation and this scenario and (ii) taken as the difference between the total land surface runoff and the red curve of *required runoff* on figure 5, therefore independent of remotely sensed estimates.
- Under these conditions, the runoff increase needed to maintain the lake level is only supplied by land runoff (surface and subsurface) by shifting the *runoff / (runoff + evaporation)* ratio.

The graph shows that the ratio from the historical simulation starts significantly below the theoretical steady lake ratio (10.2% < 17.6%) and increases progressively to 16.0% in 2019. This evolution is consistent with observations that show a progressive stabilization of the lake level (Fig. 5).

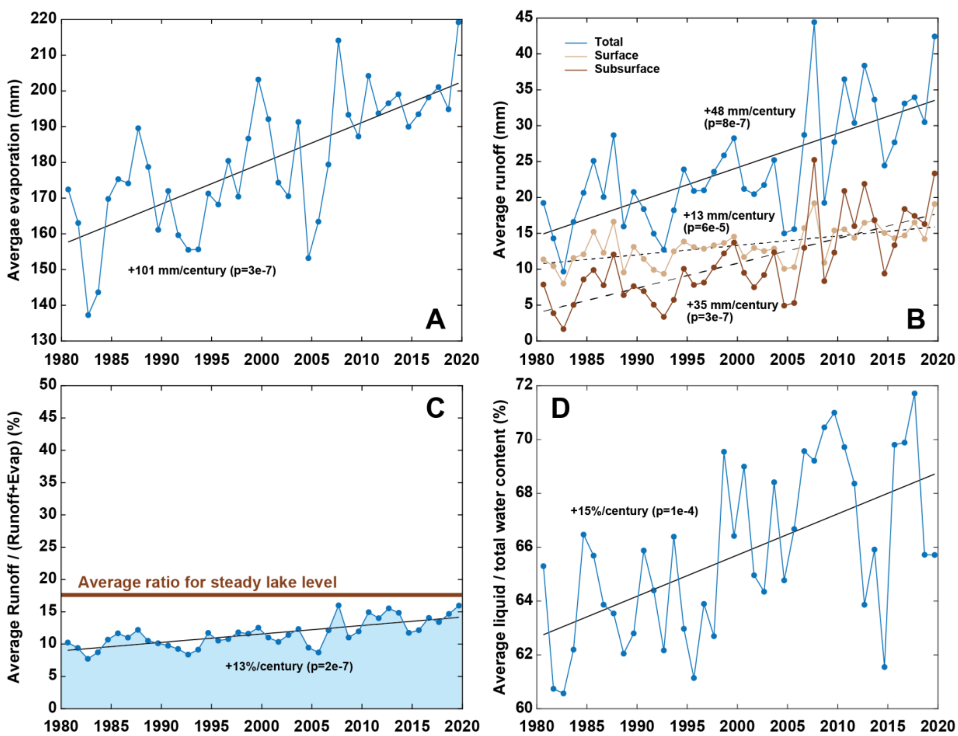

Figure 8. Hydrological results. A: yearly evaporation averaged over the whole catchment. B: yearly runoff averaged over the whole catchment. The blue curve sums the surface and subsurface runoff. C: Ratio between runoff and (evaporation + runoff) averaged over the whole catchment. The brown line indicates the theoretical average ratio needed to maintain a steady lake level when considering an identical glacier contribution to runoff (details in Sect. 4.3). D: Yearly mean of the (liquid water)/(liquid water + frozen water) ratio over the first 2 meters of ground, averaged over the whole catchment.

https://doi.org/10.5194/hess-2022-241
Preprint. Discussion started: 18 July 2022
© Author(s) 2022. CC BY 4.0 License.

Finally, Fig. 8D shows the yearly proportion of *liquid / (liquid + frozen)* water averaged for the whole catchment. The value was computed based on the daily water content (liquid and frozen) of the first 2 m of the soil column (the hydrologically active part of the column, Sect. 3.2.4) from which yearly averages were derived and used to compute a catchment scale average. The graph indicates that the proportion of liquid water in the total water content increases at around +15% per century ($p=1\times10^{-4}$), indicating an increasing availability of liquid water in the ground with time.

4.4. Thermo-hydrological couplings

Fig. 9 presents simulation results highlighting the interplay between the fluxes of energy and water at the surface and the subsurface and relating the ground temperature to the water content. Fig. 9A shows the correlation between the yearly *liquid / (liquid + frozen)* water ratio in the first 2 m of the ground and the yearly evaporation for *cold permafrost* and *warm permafrost*. The graph highlights that higher evaporation is observed during the years with higher availability of liquid water in the ground. Fig. 9B shows the correlation between the duration of the seasonal thaw and the yearly evaporation for *no permafrost* areas of the catchment. It shows that years with longer seasonal thaw tend to be associated with higher yearly evaporation.

Fig. 9C tests the relationship between the linear trend of active layer deepening and the mean evaporation (over the 40 years of simulation) for *warm permafrost* areas. Thus, this graph does not present yearly values and one point corresponds to one of the 92 simulations classified as *warm permafrost* (values based on the 40 years). The graph highlights that simulations showing an AL deepening trend are associated with low evaporation. From there, simulations with stronger evaporation show no deepening trend or even a shrinkage of the AL. This relationship is contradicted for the highest level of evaporation observed for *warm permafrost*, for which AL deepening is observed again (dark blue points of the graph). These simulations with the highest levels of evaporation also correspond to those receiving the largest amount of precipitation.

Finally, Fig. 9D displays the yearly values of subsurface runoff against the yearly average 2 m-deep temperature for disappearing permafrost. The color scale of the points indicates the time of the

https://doi.org/10.5194/hess-2022-241
Preprint. Discussion started: 18 July 2022
© Author(s) 2022. CC BY 4.0 License.

simulation. Consistent with the substantial warming trend observed for disappearing permafrost (Fig. 7A) and the increase of subsurface runoff at the catchment scale (Fig. 8B), subsurface runoff shows higher values during the year that record a positive 2 m-deep mean annual temperature. The average annual runoff when the 2 m-deep temperature is positive is 23 ± 13 mm whereas it is 2 ± 3 mm for negative 2 m-deep temperature (mean annual value).

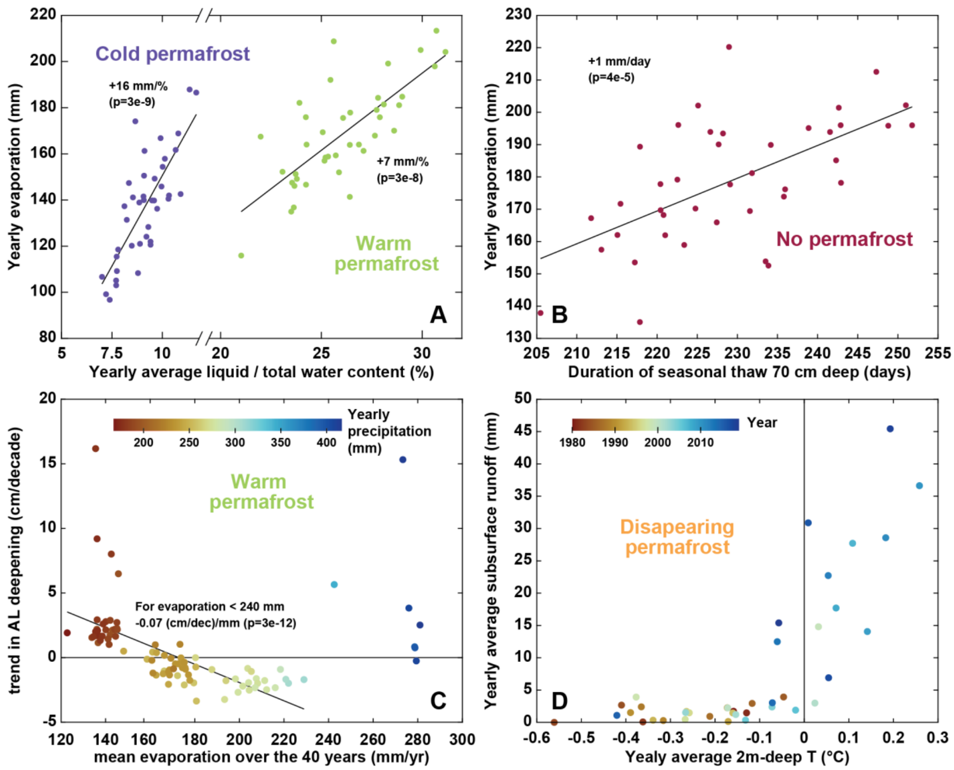

Figure 9. Thermo-hydrological couplings. A: yearly evaporation vs. yearly mean of the liquid /(liquid+frozen) water ratio over the first 2 meters of ground, averaged for simulations corresponding to cold permafrost and warm permafrost (one dot per year for each permafrost category). B: yearly evaporation vs. duration of seasonal thaw at a 70 cm depth averaged for simulations corresponding to locations without permafrost (one dot per year). C: Active layer deepening trend vs. mean evaporation over the 40 years for each simulation corresponding to warm permafrost (here one dot corresponds to one 40-years-long simulation). The color of the dots shows the precipitations averaged over the 40 years for each simulation. The linear regression excludes simulations exhibiting yearly evaporation higher than 240 mm. D: Yearly subsurface runoff vs Yearly 2 m-deep temperature averaged for simulations corresponding to locations with disappearing permafrost (one dot per year). The color of the dot indicates the year of the simulation.

5. Discussion

5.1. Limitation and potential of the approach

5.1.1. Data scarcity

The approach we develop in the present study to quantify the thermo-hydrological regime of the Paiku catchment presents both advantages and limitations that can frame discussions on the presented results. Regarding the limitations, we identify two main points. The first limitation is related to the limited amount of available field observations required to provide robust model parameterizing, climate forcing and in-depth validation of the simulations. Regarding the ground stratigraphy and parameters, in the absence of direct observations, we made use of large-scale data sets (Schaaf and Wang, 2015; Shangguan et al., 2013, 2017; Simons et al., 2020). Even though these datasets are intended to inform numerical modeling, field observation would bring additional confidence in the values we use. Regarding climatic forcing data, our AWS measurement offers sound observations to evaluate and adjust the ERA5 data processed with TopoSUB and downscaled with TopoSCALE. Yet a period of observations longer than 2 years would have brought more robust corrections and could have allowed to perform quantile mapping. Regarding the simulated temperature fields, the comparison with the loggers bring confidence that the model captures both the surface temperature mean values and seasonal patterns, but the validation exercise would benefit from additional loggers located throughout the catchment and ideally also temperature profiles from boreholes. Similarly, even though the lake evaporation values we compute finds a good agreement with those from Lei et al. (2021), a longer comparison would have brought a higher level of confidence in the values.

Finally, the lake level variations are the only hydrological observations available to evaluate the robustness of the runoff we compute. We combine lake level observations with our precipitation forcing data and lake evaporation quantifications in a simple mass conservation calculation to derive the land runoff to the lake required to reproduce the level variations (red curve on Fig. 5). The sum of the glacier and land runoff we derive over the 40 years correspond to 95% of the required runoff to the lake, indicating that the magnitude of our reconstruction is correct. Year to year comparison is less accurate and we suggest that this is the consequence of the aforementioned limitations regarding data scarcity

https://doi.org/10.5194/hess-2022-241
Preprint. Discussion started: 18 July 2022
© Author(s) 2022. CC BY 4.0 License.
Hydrology and Earth System Sciences Discussions
Open Access EGU

(including the simplifications of glacier runoff to 2 constant values over the 1980-2000 and 2000-2019 periods) and also of our modeling strategy as detailed below.

5.1.2. Modeling strategy

An important limitation in the modeling strategy we implement is the absence of water routing throughout the catchment. First, water routing could highlight physical processes that our implementation cannot represent such as the evaporation of water during its transport towards the lake, or downstream soil water content increase due to upstream runoff. In this regard, the best our approach can provide is to average these processes over time by closing the catchment water budget on the long run. We suggest that our simulations reach this goal, considering it produces 95% of the required runoff over the 40 years we study.

Second, by giving access to the timing of water transport across the catchment, water routing would allow to investigate temporal hydrological patterns at a monthly or seasonal scale. Because we work at yearly and decadal time scales, this limitation has limited consequences on our results. The main consequence is to ignore potential storage effects on the land that would delay the arrival of runoff to the lake. We suggest that this limitation contributes to explaining the limited match between computed and required runoff at a yearly time scale. Yet our subdivision of the catchment based on the different cryological states of the ground allows us to work with hydrological units that are smaller than the catchment and thus present shorter hydrological response time to precipitation.

Conversely, our approach also conveys several important advantages regarding our goal to describe and quantify the ground thermo-hydrological regime of the catchment. The use of TopoSUB enables us to produce results at a resolution of 100 x 100 m over an area of nearly 2400 km^2 with calculation costs 700 times lower than if each 100 x 100 m pixel was treated individually. Yet, thanks to the clustering method used to produce the forcing dataset (Sect. 3.2.2), the strong spatial variability of the physiography and its impact on the climate and incoming radiations is significant in the forcing data and has a major influence on the ground thermo-hydrological results, as exemplified by the strong spatial variability of ground temperatures (Fig. 6). Beyond elevation, other physiographic parameters such as aspect also influence the results. The mean values of 2 m-deep temperature and evaporation

https://doi.org/10.5194/hess-2022-241
Preprint. Discussion started: 18 July 2022
© Author(s) 2022. CC BY 4.0 License.

over the 40 years for north-facing areas (averaged over the whole catchment and over the 40 years) are of 1.3 °C and 163 mm while they reach 2.9 °C and 197 mm for the south-facing ones. This strong dependance of modeled results on physiography highlight the necessity to take it into account when modeling the thermo-hydrological regime of the ground in high mountainous environments. Finally, our approach allows us to couple the physical processes governing both energy and water fluxes at the surface and subsurface and highlight their interplay, as developed in the following section.

5.1.3. The interdependence of thermal and hydrological variables

Results presented in Sect. 4.4 highlight how water and energy fluxes at the surface and subsurface are coupled. For permafrost areas (*cold permafrost* and *warm permafrost*), evaporation shows a strong connection with the seasonal distribution between liquid and frozen water, similarly to previous modeling works for the region (Cuo et al., 2015). As such, the intensity of seasonal ground thaw plays a major role in enabling higher or lower evaporative fluxes because cold surface temperatures strongly reduce water loss from the surface and because moisture delivery to the surface is inhibited when the ground is frozen. We suggest that this dependance is particularly important in the Paiku Catchment because evaporation is strong (88% of the precipitation input to the surface evaporates on average) and because frozen water is the dominant form of water in the ground in permafrost areas (Fig. 9B, the calculation includes the first 2 meters below the surface).

Similarly, evaporation in *no permafrost* areas shows a connection with the duration of the seasonal thaw. Because frozen ground limits the evaporative fluxes, years during which the subsurface seasonal thaw is shorter are associated with reduced evaporative fluxes (Fig.9B). Runoff also shows a strong connection with the ground thermal regime and Fig. 9D highlights how changes in the ground thermal regime correspond to modifications in the hydrological pathways for *disappearing permafrost*. At the beginning of the simulation, years with 2 m-deep frozen conditions are associated with limited subsurface runoff (< 5 mm per year). Over the years, as the ground warms up and permafrost disappears, subsurface runoff increases and can reach 20 to 45 mm per year. This result is consistent with increased subsurface connectivity expected when permafrost thaws (Gao et al., 2021; Kurylyk et al., 2014) that

https://doi.org/10.5194/hess-2022-241
Preprint. Discussion started: 18 July 2022
© Author(s) 2022. CC BY 4.0 License.
Hydrology and Earth System Sciences
Open Access
Discussions

has been both observed (Chiasson-Poirier et al., 2020; Niu et al., 2016) and modeled (Gao et al., 2018; Huang et al., 2020; Lamontagne-Hallé et al., 2018).

Altogether, these results highlight the dependance of key variables quantifying the catchment hydrological balance (evaporation, runoff) to the seasonal characteristics and interannual trends of the ground thermal regime (temperature, liquid vs frozen water content). Similarly to previous studies (Ding et al., 2020; Wang and Gao, 2022), these results advocate for the necessity to couple thermal and hydrological modeling to improve our ability to understand and quantify changes in the hydrological balance of high mountain catchments. To our best knowledge, our study represents to date the most complete effort to include the variety of coupled climatological, surface and subsurface processes characterizing the climate, hydrology and ground thermal regime of high-mountain catchments in Tibet at a small scale with a high spatial resolution.

5.2. Cryo-hydrological trends in the catchment and across the QTP

5.2.1. Permafrost and ground temperature changes

Our results indicate that permafrost coverage in the Paiku catchment evolves from 27 to 22% of the land area during the simulated period. Such a coverage corresponds to sporadic permafrost (10-50% of the area) and is consistent with recent large-scale estimates of permafrost in the northern Hemisphere (Obu et al., 2019) and across the QTP (Ran et al., 2018; Zou et al., 2017). This decrease corresponds to a 19% shrinkage of the 1980 permafrost area, which is more important than the 9% reported by Gao et al. (2018), determined by catchment scale numerical modeling in the upper Heihe catchment (northeastern QTP) over a similar period. It is also slightly higher than the 13% decrease modeled from 1971 to 2015 for the Qinghai Lake catchment with a similar approach by Wang and Gao (2022). Yet it is smaller than the 34% loss modeled by Qin et al. (2017) from 1981 to 2015 for the Yellow River Source Region (YRSR, North Eastern QTP).

Active layer (AL) evolution is contrasted throughout the catchment and a deepening signal is only visible for the locations with limited evaporation (<150 mm per year). Given the strong drive of summer climate on Active Layer Thickness (ALT), this overall lack of a deepening trend highlights how evaporation can act as an energy intake at the surface, limiting the subsurface heat fluxes and thus AL

https://doi.org/10.5194/hess-2022-241
Preprint. Discussion started: 18 July 2022
© Author(s) 2022. CC BY 4.0 License.

deepening (Yang et al., 2014a). In this regard, our results fall in line with the conclusions of Fisher et al. (2016) when observing evapotranspiration and ALTs in boreal forests and also confirm the modeling experiments of Zhang et al. (2021b) on permafrost wetting in arid regions of the QTP. Besides, the lack of overall deepening trend is consistent with observations from Luo et al. (2018) in the YRSR over the last decade and with the modeled AL from Zhang et al. (2019) at the scale of the QTP for the last 40 years. Where evaporation is limited we report an AL deepening trend of 2.7 cm per decade that is smaller than the 4.8 cm per decade trend modeled by Song et al. (2020) for the YRSR for the same period and smaller than the 4.3 cm modeled by Gao et al (2018) in the upper Heihe catchment. Yet it is similar to the 2 cm per decade value modeled by Wang and Gao (2022) for the Qinghai Lake catchment from 1971 to 2015.

In *no permafrost* areas, our simulations show that the thickness of seasonal frozen ground shrinks at a rate of 6.8 cm per decade. This rate is faster than the rate of 3.1 cm per decade quantified by Qin et al. (2018) using the Stefan solution for the YRSR (1961-2016) and faster than the 3.2 cm per decade modeled by Gao et al. (2018, Heihe catchment). However, it is similar to the 6 cm per decade rate modeled by Wang and Gao (2022) in the Qinghai Lake catchment from 1971 to 2015 and smaller than the 12 cm per decade modeled by Qin et al. (2017) for the YRSR (1981-2015). All these values fall within the wide range of 3 to 29 cm per decade reported by Wang et al. (2020a) when studying seasonal frozen ground over the whole QTP with in-situ observations. Regrading timing, we report a decreasing trend of 5.3 days of frozen conditions (70 cm deep) per decade which is consistent with the decrease of 6.7 days per decade reported by Wang et al. (2020a) just below the surface.

Regarding the timing of seasonal ground thaw, our results highlight that the increase in the duration in the seasonal ground thaw (at 70 cm) is mostly driven by a progressive delay of the end date of the thaw period. This result contrasts with those from Song et al. (2020) for the same period in the YRSR who also modeled an increase in the seasonal thaw (at a 2 cm depth) but driven by an advancing trend of the start date of the seasonal thaw.

Our warming trends at a 4 m depth for permafrost areas is 0.1 °C per decade, which is substantially smaller than the 0.43 °C per decade observed at this depth between 1996 and 2006 in permafrost boreholes along the Qinghai-Tibetan Highway in the North East of the QTP (Wu and Zhang, 2008).

© Author(s) 2022. CC BY 4.0 License.

Zhang et al. (2019) reported a 1.3 °C per decade of warming of the permafrost top during winter that is consistent with the trend of 1.4 °C per decade we observe at 2 m depth (mean AL between 1.4 and 1.7 m in our simulations) for the months of December, January and February.

5.2.2. Evaporation and runoff changes

Our results are characterized by (i) an increase of both evaporation and runoff (Fig. 8), mainly driven by an increase in precipitation (Fig. 3), (ii) a runoff/(runoff+evaporation) ratio exhibiting an increasing trend as a result of ground warming and permafrost disappearance that both enable more subsurface runoff along time (Fig. 8 and 9) and (iii) an increase in the proportion of liquid water in the ground compared to ice. Regarding all these points, our results find a good consistency with the evolution reported by Gao et al. (2018) for the upper Heihe catchment (northeastern QTP) using a similar approach for a comparable period (1971-2013). The increasing trends in evaporation and runoff they report for the thawing season (dominant period for both processes) are comparable with the yearly values we report: +100 mm cm^{-1} for evaporation (our study: +101 mm per century) and +33 mm per century for runoff (our study: +48 mm per century). Similar evolutions are also reported by Wang and Gao (2022) for the Qinghai Lake catchment and by Qin et al. (2017) for the YRSR (1981-2015). Regarding differences, Qin et al. (2017) modeled a stronger evaporation increase (143 mm per century) linked to a decreasing runoff coefficient. Similarly to Li et al. (2019), we see that an important part of snow melt (49%) infiltrates in the ground and later contributes to runoff and evaporation.

5.3. Evaporation vs runoff and sensitivity to climate conditions

Our results indicate that evaporation is particularly strong in the Paiku catchment. Over the 40 years of simulation, 10% of the total precipitation is converted to runoff, the rest of the water is either directly returned to the atmosphere from the snowpack via snow sublimation or from the ground surface via evaporation. Comparatively, Gao et al. (2018) observed and modeled a ratio of around 35% for the Heihe catchment; Qin et al. (2017) reported an average ratio of 33% for the YRSR and Li et al. (2014) a ratio of 83% for the Qugaqie catchment (central QTP) but modeling hydrological fluxes only.

The role of permafrost regarding the runoff/evaporation distribution is a complex question (Bring et al., 2016). Some studies have suggested that landscape-scale permafrost thaw would trigger more

https://doi.org/10.5194/hess-2022-241
Preprint. Discussion started: 18 July 2022
© Author(s) 2022. CC BY 4.0 License.

evaporation (Walvoord and Kurylyk, 2016, Fig. 4). This phenomenon was modeled by Wang et al. (2018) in the upper Heihe River Catchment for which they reported that the thickening of the active layer increased the ground storage capacity and led to a decrease in runoff and an increase in evapotranspiration. Studying evaporation at the scale of the whole Tibetan plateau, Wang et al. (2020b) also reported that permafrost thawing accelerated evapotranspiration (1961-2014).

Conversely, Zhang et al. (2003) and Carey and Woo, (1999) reported that shallow frozen ground conditions (such as a shallow active layer) maintain higher water contents close to the surface, promoting higher evaporation. Sjöberg et al. (2021) modeled this phenomenon with a fully coupled cryo-hydrological model including surface energy balance calculation. They modeled a slope with a simplified geometry in 2D for different permafrost coverages. They found that hillslopes with continuous permafrost have twice as high rates of evapotranspiration compared to hillslopes with no permafrost.

As such, the interplay between the runoff/evaporation distribution and the ground thermal regime in areas where permafrost coverage shows a spatiotemporal variability is difficult to apprehend. This complexity is most likely due to a strong sensitivity to the drainage conditions (fast flows of steep mountain environments vs. slow flows of lowland catchments) and to the climate setting, both at the annual scale (arid regions vs. wet regions) and at the seasonal time scale (relative timing of temperature variations, rainfall, snowfall, snow melt and ground freeze/thaw).

To further understand this question in the case of the Paiku catchment, we conducted a simple sensitivity test on the climatic conditions. We ran the same 40 years of simulations (with thermal initialization) for a climate 1 °C cooler and 30% wetter (more precipitation) than the historical scenario. We call this new scenario *colder and wetter* (to be compared with the *historical scenario*, i.e. the results of the present study presented in Sect. 4). Results of this experiment are presented in Fig. 10. Because of the difference in climate forcing, the *colder and wetter* scenario produced a greater amount of *cold* and *warm permafrost* areas than the historical scenario, as presented on Fig. 10A. Fig. 10B shows the proportion of the precipitation reaching the surface (rain + snow – snow sublimation) that produces runoff compared to evaporation for the Paiku catchment.

https://doi.org/10.5194/hess-2022-241
Preprint. Discussion started: 18 July 2022
© Author(s) 2022. CC BY 4.0 License.

Hydrology and Earth System Sciences
Discussions

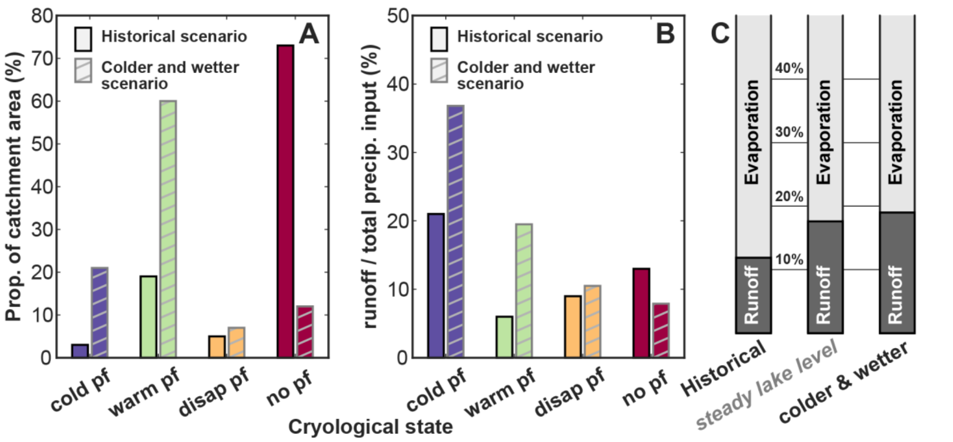

Figure 10. Sensitivity of the distribution between runoff and evaporation to climate. A: distribution of the different cryological states of the ground for the historical scenario (presented in Section 4) and for an alternative scenario where the climate is 1 °C colder and brings 30% more precipitation. B: runoff as a proportion of the precipitation input to the land (rainfall + snowfall – snow sublimation) for the different cryological states of the ground and for the 2 climatic scenarios. C: catchment scale ratio between runoff and evaporation for (i) the historical scenario, (ii) for a steady lake level with the same glacier contribution (same as Fig. 8 bottom left) and (iii) for the colder and wetter scenario.

The *historical scenario* shows that *cold permafrost* areas produces the highest proportion of runoff, which we attribute to the fact that the ground in these areas is most of the time frozen, turning a substantial part of the snow melt and rainfall into surface runoff. When considering grounds with a hydrologically active subsurface (*warm permafrost*, *disappearing permafrost* and *no permafrost*) in the historical scenario, the proportion of runoff increases slightly from *warm permafrost* to *no permafrost*. Such an evolution then corroborates the idea that the presence of permafrost tends to increase evaporation at the expense of runoff, as modeled by Sjöberg et al. (2021). Yet, for the *colder and wetter* scenario, runoff shows a regular decrease from *cold* to *no permafrost* with a more pronounced trend than the historical scenario. Several factors can be at play in this transition and most likely involve (i) a different extent and altitudinal distribution for each cryological types of ground, (ii) a reduced intensity of evaporation due to cooler surface temperatures, (iii) a higher soil water content driven by higher precipitation and (iv) difference in the seasonal timings as listed earlier. Altogether, these processes substantially change the proportion of water that ends up as runoff water available for the lake, as highlighted by Fig. 10C.

https://doi.org/10.5194/hess-2022-241
Preprint. Discussion started: 18 July 2022
© Author(s) 2022. CC BY 4.0 License.

5.4. Implications for lake level changes over the QTP

At the scale of the Paiku catchment and in regard of lake level variations, the results we present highlight that:

- The sum of the direct precipitation in the lake, the land runoff and the glacier runoff are not enough to compensate the lake evaporation over the study period, hence leading to the observed lake level decrease.
- Long term hydrological trends in the catchment are led by trends in the climate, as precipitation increase both drives an evaporation and runoff increase over the 40 years.
- Ground thermal changes increase the distribution of liquid vs. frozen water in the ground and the duration of seasonal thaw, both directly affecting evaporation and runoff towards the lake.
- Ground warming and permafrost thawing promote subsurface runoff over time, contributing to increase the runoff/evaporation ratio of the catchment.
- Over the last 40 years, the presence of permafrost seems to promote evaporation at the expense of runoff. Yet this trend appears to be climate-dependent and the cryological state of the ground might shift the runoff/evaporation distribution in the other direction under colder and wetter climates.

At the scale of the QTP, these results have several implications. First, a better understanding of the recent and future lake level variations will come with a better knowledge of spatial patterns and temporal trends in precipitation. Second, climate changes are modifying the ground thermal regime of Tibetan catchments through active layer deepening and changes in the seasonal freeze/thaw cycles, affecting evaporation, runoff volumes and pathways and overall, changing the hydrological functioning of Tibetan catchments (and the waterflow provided to the lakes). Finally, the effect of permafrost on the distribution between evaporation and runoff seems to be dependent on the climate settings and the permafrost coverage of the catchment. Because it can both promote evaporation or runoff depending on the setting, the ground thermal regime of the catchment seems to have the possibility to create a positive feedback both towards lake level decrease or increase. Further studies could therefore focus on comparing the thermo-hydrological regime of different Tibetan catchments with contrasted lake level changes and permafrost coverage, to test to which extent these differences can explain the spatial patterns of lake level changes across the QTP.

6. Conclusion

We confirm that the Paiku catchment presents different types of ground cryological state from seasonal frozen ground to permafrost. Permafrost coverage shrinks from 27 to 22% of the land area from the 1980s to the 2010s (19% loss of permafrost area). The whole catchment warms up at a rate of 1.7 °C per century (2 m deep), with a substantial elevation-dependent variability. This warming is concomitant with an increase in the duration of the seasonal thaw, mainly supported by a progressive delay of the end date of the thaw period. Where permafrost is present, active layer deepening is only observed where evaporation is limited (<150 mm yr^{-1}).

Over the simulation period, we also report an increase in evaporation (+101 mm per century), surface and subsurface runoff (+13 and +35 mm per century respectively). Together, this leads towards an increase of the runoff/(runoff + evaporation) ratio of +13% per century. These results highlight the strong interdependence between the ground thermal and hydrological regimes and the necessity to jointly represent them to accurately quantify evaporation and runoff in this type of environment. Indeed, we show that ground thermal changes increase the availability of liquid water in the ground and the duration of seasonal thaw and that both directly affect evaporation and runoff towards the lake. Additionally, permafrost thawing and ground warming promote subsurface runoff over time, contributing to increase the runoff/evaporation ratio of the catchment.

Over the last 40 years, the presence of permafrost seems to promote evaporation at the expense of runoff. Yet this trend appears to be climate-dependent and the cryological state of the ground might shift the runoff/evaporation distribution in the other direction under colder and wetter climates. Further studies should investigate this phenomenon and how it might contribute to explain the contrasted lake level evolutions across the QTP.

https://doi.org/10.5194/hess-2022-241
Preprint. Discussion started: 18 July 2022
© Author(s) 2022. CC BY 4.0 License.

771 # Appendix A: model parameters

772 *Table A. Parameters of the model.*

Depth	Layer	Parameter	Values	Source	Calculation
0.0 m	Surface	**Albedo**	**0.24**	Modis MCD43A3.006	November mean, 4600-5100 masl
		Emissivity	**0.95**	Modis MCD43A3.006	November mean, 4600-5100 masl
		Roughness	**0.024**	-	Adjusted to fit loggers T values
0.0 m	Top soil	**Thickness**	**0.30 m**	HiHydro Soil v1.0	modeling framework
		Porosity	**0.5**	Shanggguann et al. 2013	mean
		Organic	**8.60%**	HiHydro Soil v1.0	catchment mean
		Mineral	**41.40%**	-	substraction (100 - porosity - orga)
0.3 m		**Soil type**	**Sand**	Shanggguann et al. 2013	dominant fraction
		Field capacity	**0.32**	HiHydro Soil v1.0	catchment mean
		Hydro cond	**0.000030 m s^{-1}**	HiHydro Soil v1.0	catchment mean
		Alpha	**0.028 cm^{-1}**	HiHydro Soil v1.0	catchment mean
0.3 m		**n**	**1.481**	HiHydro Soil v1.0	catchment mean
0.3 m	Bottom soil	**Thickness**	**1.70 m**	Shangguan et al. 2017	truncation, consistent with litterature
		Porosity	**0.4**	Shanggguann et al. 2013	catchment mean
		Organic	**4.20%**	HiHydro Soil v1.0	catchment mean
		Mineral	**55.80%**	-	substraction (100 - porosity - orga)
1.7 m		**Soil type**	**Sand**	Shanggguann et al. 2013	dominant fraction
		Field capacity	**0.32**	HiHydro Soil v1.0	catchment mean
		Hydro cond	**0.000016 m s^{-1}**	HiHydro Soil v1.0	catchment mean
		Alpha	**0.062 cm^{-1}**	HiHydro Soil v1.0	catchment mean
2.0 m		**n**	**1.707**	HiHydro Soil v1.0	catchment mean
2.0 m	Bedrock	**Thickness**	**98.3 m**	-	-
		Porosity	**0.03**	-	-
98 m		**Organic**	**0%**	-	-
		Mineral	**97%**	-	-
		Soil type	**Sand**	-	-
100 m		**Field Capacity**	**0.03**	-	equal to porosity

773

https://doi.org/10.5194/hess-2022-241
Preprint. Discussion started: 18 July 2022
© Author(s) 2022. CC BY 4.0 License.

Hydrology and Earth System Sciences
Discussions
Open Access
EGU

Appendix B: Geological map of the catchment

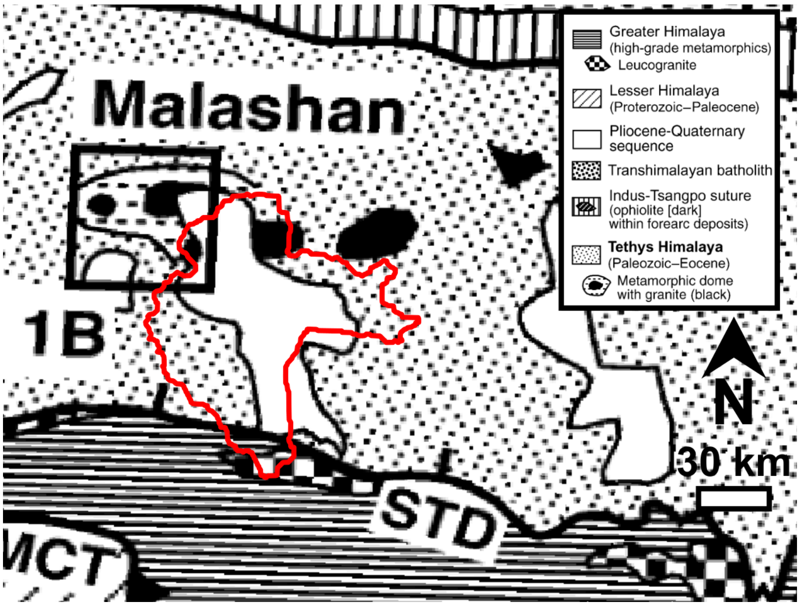

Figure B. Geology of the catchment. Modified from Aoya et al. (2015). The red contour indicates the limits of the Paiku catchment.

Appendix C: TopoSUB subsampling of the catchment

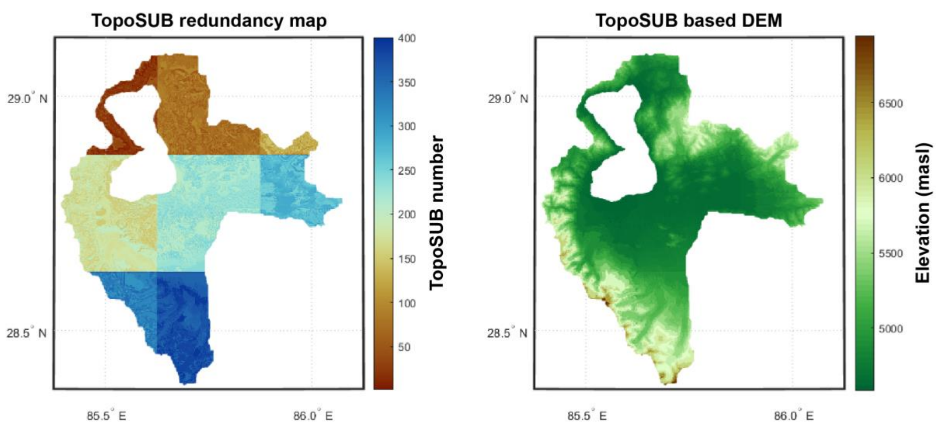

Figure C. Application of the TopoSUB clustering method (Fiddes and Gruber, 2012) in the Paiku catchment. Left: number of the TopoSUB points. Strong color changes reflect the footprint of the 8 ERA5 pixels that the catchment intersects. Small color changes within a given of these zones show the distribution of the 50 TopoSUB points covering each tile (Sect. 3.2.2.) B: topographic map reconstructed from the TopoSUB approach.

https://doi.org/10.5194/hess-2022-241
Preprint. Discussion started: 18 July 2022
© Author(s) 2022. CC BY 4.0 License.

Hydrology and Earth System Sciences
Discussions

Appendix D: Evaluation of forcing data

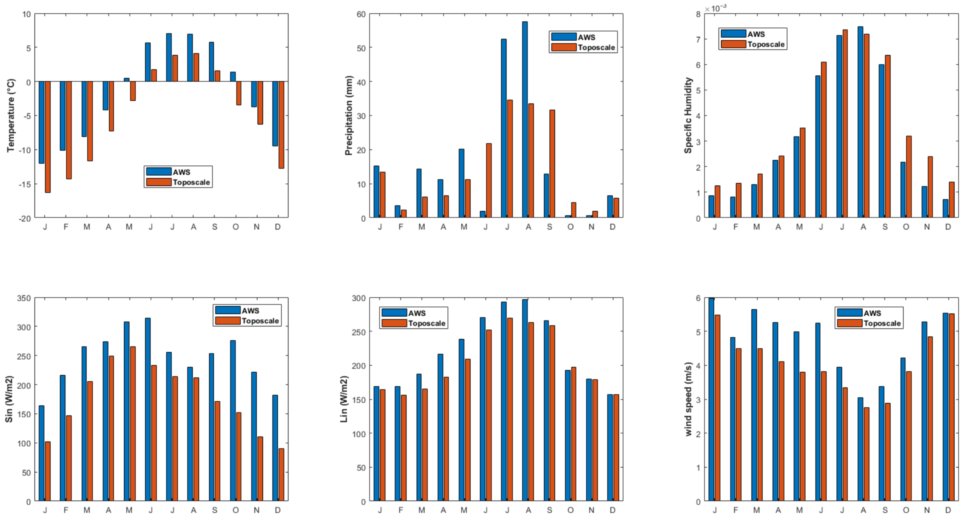

Figure D. Comparison between the AWS data and the model forcing data downscaled from ERA5 with the TopoSCALE and TopoSUB approaches. Based on the AWS data, a monthly correction factor is applied to the downscaled data so that monthly data matches for the observed period for each variable (methodological details in Sect. 3.2.2.).

Appendix E: Seasonal frozen ground

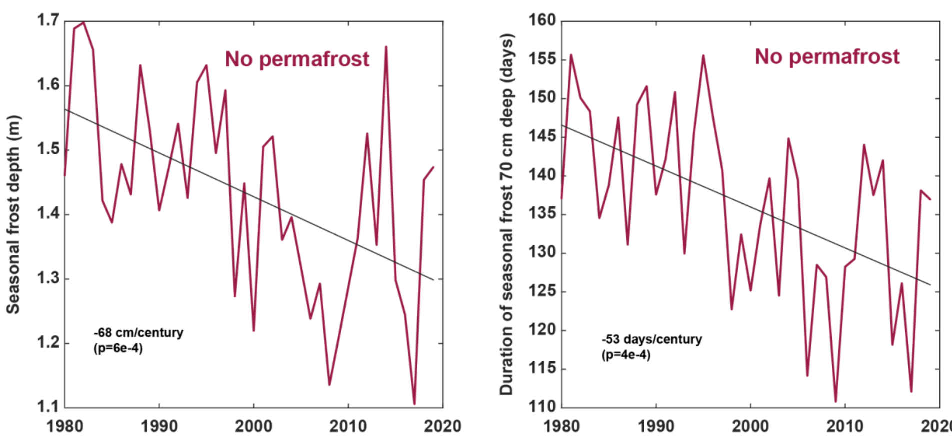

Figure E. Temporal trends for seasonal frozen ground where there is no permafrost. Simulations presenting occurrences of persisting thawed conditions from one year to another were excluded. The presented curves average thus 88% of the total permafrost-free areas of the catchment.

https://doi.org/10.5194/hess-2022-241
Preprint. Discussion started: 18 July 2022
© Author(s) 2022. CC BY 4.0 License.

Hydrology and Earth System Sciences
Discussions
Open Access

797 # Appendix F: Cryological state of the ground

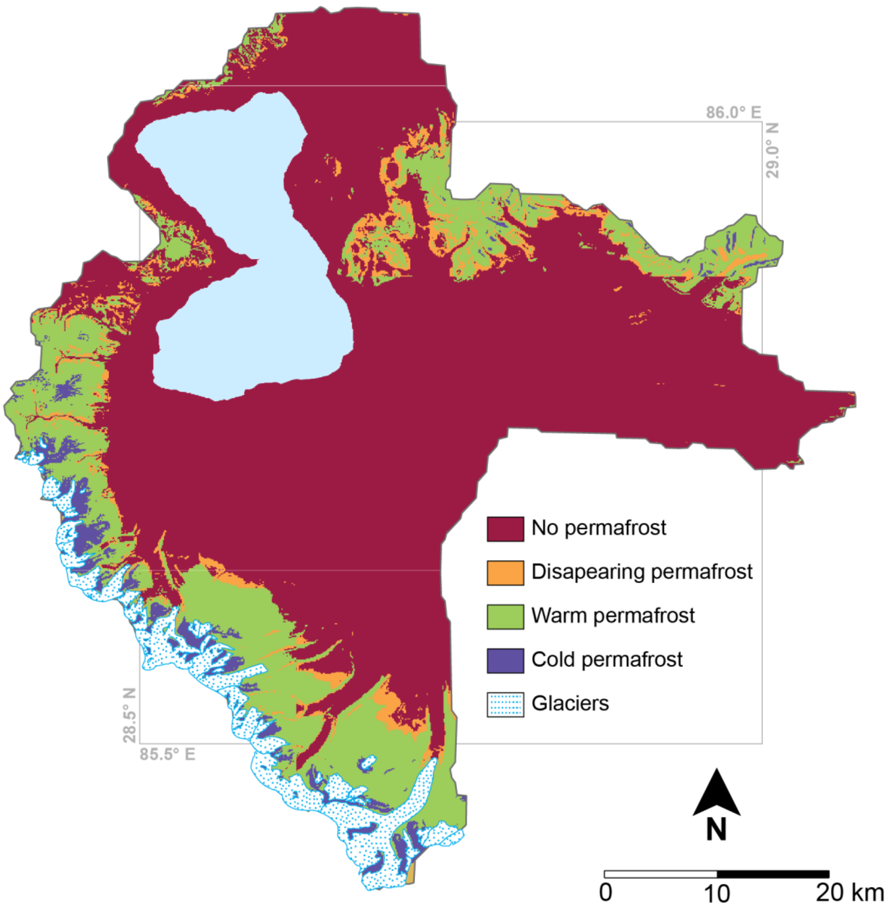

798
799 *Figure F. Cryological state of the ground. See methodological descriptions in Sect. 4.2.*

https://doi.org/10.5194/hess-2022-241
Preprint. Discussion started: 18 July 2022
© Author(s) 2022. CC BY 4.0 License.

Hydrology and Earth System Sciences
Discussions

Code availability. The CryoGrid community model (version 1.0) and related documentation are available at: https://github.com/CryoGrid/CryoGridCommunity_source.

Data availability. Field data will be permanently deposited on XXX upon acceptance of the manuscript.

Author contribution. L.M, W. I. and S.W. designed the study. L.M. and M.M. conducted the numerical simulations. S.W., M.L. and L.M. contributed to the model development. F.B., W.I., Y.L. ad S.A. acquired field data. L.M., F.B., M.M., P.K., Y.L. and T.M. analyzed and processed the data. J.F. provided downscaled forcing data for the model. All authors contributed to result interpretation and to manuscript preparation.

Competing interests. The authors declare that they have no conflict of interest.

Acknowledgements. This study was funded by the open program of the Dutch Research Council (NWO) (ALWOP.467) and by the Strategic Priority Research Program of the Chinese Academy of Sciences within the Pan-Third Pole Environment framework (grant agreement no. XDA20100300). The land surface and lake simulations were performed on Utrecht Geosciences computer cluster. Sebastian Westermann acknowledges funding by European Space Agency Permafrost_CCI (https://climate.esa.int/en/projects/permafrost/).

https://doi.org/10.5194/hess-2022-241
Preprint. Discussion started: 18 July 2022
© Author(s) 2022. CC BY 4.0 License.

References

Aoya, M., Wallis, S. R., Terada, K., Lee, J., Kawakami, T., Wang, Y. and Heizler, M.: North-south extension in the Tibetan crust triggered by granite emplacement, Geology, 33(11), 853, doi:10.1130/G21806.1, 2005.

Bhattacharya, A., Bolch, T., Mukherjee, K., King, O., Menounos, B., Kapitsa, V., Neckel, N., Yang, W. and Yao, T.: High Mountain Asian glacier response to climate revealed by multi-temporal satellite observations since the 1960s, Nat. Commun., 12(1), 4133, doi:10.1038/s41467-021-24180-y, 2021.

Bibi, S., Wang, L., Li, X., Zhou, J., Chen, D. and Yao, T.: Climatic and associated cryospheric, biospheric, and hydrological changes on the Tibetan Plateau: a review, Int. J. Climatol., 38(January), e1–e17, doi:10.1002/joc.5411, 2018.

Bolch, T., Shea, J. M., Liu, S., Azam, F. M., Gao, Y., Gruber, S., Immerzeel, W. W., Kulkarni, A., Li, H., Tahir, A. A., Zhang, G. and Zhang, Y.: Status and Change of the Cryosphere in the Extended Hindu Kush Himalaya Region, in The Hindu Kush Himalaya Assessment: Mountains, Climate Change, Sustainability and People, edited by P. Wester, A. Mishra, A. Mukherji, and A. B. Shrestha, pp. 209–255, Springer International Publishing, Cham., 2019.

Bring, A., Fedorova, I., Dibike, Y., Hinzman, L., Mård, J., Mernild, S. H., Prowse, T., Semenova, O., Stuefer, S. L. and Woo, M. -K.: Arctic terrestrial hydrology: A synthesis of processes, regional effects, and research challenges, J. Geophys. Res. Biogeosciences, 121(3), 621–649, doi:10.1002/2015JG003131, 2016.

Brun, F., Berthier, E., Wagnon, P., Kääb, A. and Treichler, D.: A spatially resolved estimate of High Mountain Asia glacier mass balances from 2000 to 2016, Nat. Geosci., 10(9), 668–673, doi:10.1038/ngeo2999, 2017.

Brun, F., Treichler, D., Shean, D. and Immerzeel, W. W.: Limited Contribution of Glacier Mass Loss to the Recent Increase in Tibetan Plateau Lake Volume, Front. Earth Sci., 8(November), 1–14, doi:10.3389/feart.2020.582060, 2020.

Cao, J., Qin, D., Kang, E. and Li, Y.: River discharge changes in the Qinghai-Tibet Plateau, Chinese Sci. Bull., 51(5), 594–600, doi:10.1007/s11434-006-0594-6, 2006.

Carey, S. K. and Woo, M.-K.: Hydrology of two slopes in subarctic Yukon, Canada, Hydrol. Process., 13(16), 2549–2562, doi:10.1002/(SICI)1099-1085(199911)13:16<2549::AID-HYP938>3.0.CO;2-H, 1999.

Carey, S. K. and Woo, M.: Spatial variability of hillslope water balance, wolf creek basin, subarctic yukon, Hydrol. Process., 15(16), 3113–3132, doi:10.1002/hyp.319, 2001.

Chen, R., Wang, G., Yang, Y., Liu, J., Han, C., Song, Y., Liu, Z. and Kang, E.: Effects of Cryospheric Change on Alpine Hydrology: Combining a Model With Observations in the Upper Reaches of the Hei River, China, J. Geophys. Res. Atmos., 123(7), 3414–3442, doi:10.1002/2017JD027876, 2018.

Cheng, G. and Jin, H.: Permafrost and groundwater on the Qinghai-Tibet Plateau and in northeast China, Hydrogeol. J., 21(1), 5–23, doi:10.1007/s10040-012-0927-2, 2013.

Chiasson-Poirier, G., Franssen, J., Lafrenière, M. J., Fortier, D. and Lamoureux, S. F.: Seasonal evolution of active layer thaw depth and hillslope-stream connectivity in a permafrost watershed, Water Resour. Res., 56(1), 1–18, doi:10.1029/2019WR025828, 2020.

Cuo, L., Zhang, Y., Bohn, T. J., Zhao, L., Li, J., Liu, Q. and Zhou, B.: Frozen soil degradation and its effects on surface hydrology in the northern Tibetan Plateau, J. Geophys. Res. Atmos., 120(16), 8276–8298, doi:10.1002/2015JD023193, 2015.

Dall'Amico, M., Endrizzi, S., Gruber, S. and Rigon, R.: A robust and energy-conserving model of freezing variably-saturated soil, Cryosph., 5(2), 469–484, doi:10.5194/tc-5-469-2011, 2011.

Ding, Y., Zhang, S., Chen, R., Han, T., Han, H., Wu, J., Li, X., Zhao, Q., Shangguan, D., Yang, Y., Liu, J., Wang, S., Qin, J. and Chang, Y.: Hydrological Basis and Discipline System of Cryohydrology: From a Perspective of Cryospheric Science, Front. Earth Sci., 8(December), 1–12, doi:10.3389/feart.2020.574707, 2020.

Fiddes, J. and Gruber, S.: TopoSUB: A tool for efficient large area numerical modelling in complex topography at sub-grid scales, Geosci. Model Dev., 5(5), 1245–1257, doi:10.5194/gmd-5-1245-2012, 2012.

Fiddes, J. and Gruber, S.: TopoSCALE v.1.0: downscaling gridded climate data in complex terrain, Geosci. Model Dev., 7(1), 387–405, doi:10.5194/gmd-7-387-2014, 2014.

https://doi.org/10.5194/hess-2022-241
Preprint. Discussion started: 18 July 2022
© Author(s) 2022. CC BY 4.0 License.

Hydrology and Earth System Sciences
Open Access
EGU
Discussions

Fisher, J. P., Estop-Aragonés, C., Thierry, A., Charman, D. J., Wolfe, S. A., Hartley, I. P., Murton, J. B., Williams, M. and Phoenix, G. K.: The influence of vegetation and soil characteristics on active-layer thickness of permafrost soils in boreal forest, Glob. Chang. Biol., 22(9), 3127–3140, doi:10.1111/gcb.13248, 2016.

Gao, B., Yang, D., Qin, Y., Wang, Y., Li, H., Zhang, Y. and Zhang, T.: Change in frozen soils and its effect on regional hydrology, upper Heihe basin, northeastern Qinghai-Tibetan Plateau, Cryosphere, 12(2), 657–673, doi:10.5194/tc-12-657-2018, 2018.

Gao, H., Wang, J., Yang, Y., Pan, X., Ding, Y. and Duan, Z.: Permafrost Hydrology of the Qinghai-Tibet Plateau: A Review of Processes and Modeling, Front. Earth Sci., 8(January), 1–13, doi:10.3389/feart.2020.576838, 2021.

van Genuchten, M. T.: A Closed-form Equation for Predicting the Hydraulic Conductivity of Unsaturated Soils, Soil Sci. Soc. Am. J., 44(5), 892–898, doi:10.2136/sssaj1980.03615995004400050002x, 1980.

Hersbach, H., Bell, B., Berrisford, P., Hirahara, S., Horányi, A., Muñoz-Sabater, J., Nicolas, J., Peubey, C., Radu, R., Schepers, D., Simmons, A., Soci, C., Abdalla, S., Abellan, X., Balsamo, G., Bechtold, P., Biavati, G., Bidlot, J., Bonavita, M., Chiara, G., Dahlgren, P., Dee, D., Diamantakis, M., Dragani, R., Flemming, J., Forbes, R., Fuentes, M., Geer, A., Haimberger, L., Healy, S., Hogan, R. J., Hólm, E., Janisková, M., Keeley, S., Laloyaux, P., Lopez, P., Lupu, C., Radnoti, G., Rosnay, P., Rozum, I., Vamborg, F., Villaume, S. and Thépaut, J.: The ERA5 global reanalysis, Q. J. R. Meteorol. Soc., 146(730), 1999–2049, doi:10.1002/qj.3803, 2020.

Hu, G.-R., Li, X.-Y. and Yang, X.-F.: The impact of micro-topography on the interplay of critical zone architecture and hydrological processes at the hillslope scale: Integrated geophysical and hydrological experiments on the Qinghai-Tibet Plateau, J. Hydrol., 583(January), 124618, doi:10.1016/j.jhydrol.2020.124618, 2020.

Huang, K., Dai, J., Wang, G., Chang, J., Lu, Y., Song, C., Hu, Z., Ahmed, N. and Ye, R.: The impact of land surface temperatures on suprapermafrost groundwater on the central Qinghai-Tibet Plateau, Hydrol. Process., 34(6), 1475–1488, doi:10.1002/hyp.13677, 2020.

Hugonnet, R., McNabb, R., Berthier, E., Menounos, B., Nuth, C., Girod, L., Farinotti, D., Huss, M., Dussaillant, I., Brun, F. and Kääb, A.: Accelerated global glacier mass loss in the early twenty-first century, Nature, 592(7856), 726–731, doi:10.1038/s41586-021-03436-z, 2021.

IPCC: IPCC Special Report on the Ocean and Cryosphere in a Changing Climate, Intergov. Panel Clim. Chang., undefined [online] Available from: https://www.ipcc.ch/srocc/chapter/summary-for-policymakers/, 2019.

Jiang, H., Yang, Y., Bai, Y. and Wang, H.: Evaluation of the Total, Direct, and Diffuse Solar Radiations From the ERA5 Reanalysis Data in China, IEEE Geosci. Remote Sens. Lett., 17(1), 47–51, doi:10.1109/LGRS.2019.2916410, 2020.

Jiang, Q., Li, W., Fan, Z., He, X., Sun, W., Chen, S., Wen, J., Gao, J. and Wang, J.: Evaluation of the ERA5 reanalysis precipitation dataset over Chinese Mainland, J. Hydrol., 595(September 2020), 125660, doi:10.1016/j.jhydrol.2020.125660, 2021.

Jiao, D., Xu, N., Yang, F. and Xu, K.: Evaluation of spatial-temporal variation performance of ERA5 precipitation data in China, Sci. Rep., 11(1), 17956, doi:10.1038/s41598-021-97432-y, 2021.

King, O., Bhattacharya, A., Bhambri, R. and Bolch, T.: Glacial lakes exacerbate Himalayan glacier mass loss, Sci. Rep., 9(1), 18145, doi:10.1038/s41598-019-53733-x, 2019.

Koren, V., Schaake, J., Mitchell, K., Duan, Q.-Y., Chen, F. and Baker, J. M.: A parameterization of snowpack and frozen ground intended for NCEP weather and climate models, J. Geophys. Res. Atmos., 104(D16), 19569–19585, doi:10.1029/1999JD900232, 1999.

Kurylyk, B. L., MacQuarrie, K. T. B. and McKenzie, J. M.: Climate change impacts on groundwater and soil temperatures in cold and temperate regions: Implications, mathematical theory, and emerging simulation tools, Earth-Science Rev., 138, 313–334, doi:10.1016/j.earscirev.2014.06.006, 2014.

Lamontagne-Hallé, P., McKenzie, J. M., Kurylyk, B. L. and Zipper, S. C.: Changing groundwater discharge dynamics in permafrost regions, Environ. Res. Lett., 13(8), 084017, doi:10.1088/1748-9326/aad404, 2018.

Langer, M., Westermann, S., Boike, J., Kirillin, G., Grosse, G., Peng, S. and Krinner, G.: Rapid degradation of permafrost underneath waterbodies in tundra landscapes-Toward a representation of thermokarst in land surface models, J. Geophys. Res. Earth Surf., 121(12), 2446–2470, doi:10.1002/2016JF003956, 2016.

Lei, Y., Yao, T., Bird, B. W., Yang, K., Zhai, J. and Sheng, Y.: Coherent lake growth on the central Tibetan Plateau since the 1970s: Characterization and attribution, J. Hydrol., 483, 61–67, doi:10.1016/j.jhydrol.2013.01.003,

Hydrology and Earth System Sciences
Open Access
Discussions

2013.

Lei, Y., Yang, K., Wang, B., Sheng, Y., Bird, B. W., Zhang, G. and Tian, L.: Response of inland lake dynamics over the Tibetan Plateau to climate change, Clim. Change, 125(2), 281–290, doi:10.1007/s10584-014-1175-3, 2014.

Lei, Y., Yao, T., Yang, K., Bird, B. W., Tian, L., Zhang, X., Wang, W., Xiang, Y., Dai, Y., Lazhu, Zhou, J. and Wang, L.: An integrated investigation of lake storage and water level changes in the Paiku Co basin, central Himalayas, J. Hydrol., 562(May), 599–608, doi:10.1016/j.jhydrol.2018.05.040, 2018.

Lei, Y., Yao, T., Yang, K., Ma, Y. and Bird, B. W.: Contrasting hydrological and thermal intensities determine seasonal lake-level variations – a case study at Paiku Co on the southern Tibetan Plateau, Hydrol. Earth Syst. Sci., 25(6), 3163–3177, doi:10.5194/hess-25-3163-2021, 2021.

Li, B., Yu, Z., Liang, Z. and Acharya, K.: Hydrologic response of a high altitude glacierized basin in the central Tibetan Plateau, Glob. Planet. Change, 118, 69–84, doi:10.1016/j.gloplacha.2014.04.006, 2014.

Li, H., Li, X., Yang, D., Wang, J., Gao, B., Pan, X., Zhang, Y. and Hao, X.: Tracing Snowmelt Paths in an Integrated Hydrological Model for Understanding Seasonal Snowmelt Contribution at Basin Scale, J. Geophys. Res. Atmos., 124(16), 8874–8895, doi:10.1029/2019JD030760, 2019.

Luo, D., Jin, H., Wu, Q., Bense, V. F., He, R., Ma, Q., Gao, S., Jin, X. and Lü, L.: Thermal regime of warm-dry permafrost in relation to ground surface temperature in the Source Areas of the Yangtze and Yellow rivers on the Qinghai-Tibet Plateau, SW China, Sci. Total Environ., 618, 1033–1045, doi:10.1016/j.scitotenv.2017.09.083, 2018.

Luo, D., Jin, H., Bense, V. F., Jin, X. and Li, X.: Hydrothermal processes of near-surface warm permafrost in response to strong precipitation events in the Headwater Area of the Yellow River, Tibetan Plateau, Geoderma, 376(May), 114531, doi:10.1016/j.geoderma.2020.114531, 2020.

Magnin, F., Josnin, J.-Y., Ravanel, L., Pergaud, J., Pohl, B. and Deline, P.: Modelling rock wall permafrost degradation in the Mont Blanc massif from the LIA to the end of the 21st century, Cryosph., 11(4), 1813–1834, doi:10.5194/tc-11-1813-2017, 2017.

Martin, L. C. P., Nitzbon, J., Aas, K. S. S., Etzelmüller, B., Kristiansen, H. and Westermann, S.: Stability Conditions of Peat Plateaus and Palsas in Northern Norway, J. Geophys. Res. Earth Surf., 124(3), 705–719, doi:10.1029/2018JF004945, 2019.

Maurer, J. M., Schaefer, J. M., Rupper, S. and Corley, A.: Acceleration of ice loss across the Himalayas over the past 40 years, Sci. Adv., 5(6), doi:10.1126/sciadv.aav7266, 2019.

Monin, A. S. and Obukhov, A. M.: Basic laws of turbulent mixing in the surface layer of the atmosphere, Contrib. Geophys. Inst. Acad. Sci. USSR, 151, 163–187, 1954.

Mualem, Y.: A new model for predicting the hydraulic conductivity of unsaturated porous media, Water Resour. Res., 12(3), 513–522, doi:10.1029/WR012i003p00513, 1976.

Nakano, Y. and Brown, J.: Mathematical Modeling and Validation of the Thermal Regimes in Tundra Soils, Barrow, Alaska, Arct. Alp. Res., 4(1), 19, doi:10.2307/1550211, 1972.

Niu, L., Ye, B., Li, J. and Sheng, Y.: Effect of permafrost degradation on hydrological processes in typical basins with various permafrost coverage in Western China, Sci. China Earth Sci., 54(4), 615–624, doi:10.1007/s11430-010-4073-1, 2011.

Niu, L., Ye, B., Ding, Y., Li, J., Zhang, Y., Sheng, Y. and Yue, G.: Response of hydrological processes to permafrost degradation from 1980 to 2009 in the Upper Yellow River Basin, China, Hydrol. Res., 47(5), 1014–1024, doi:10.2166/nh.2016.096, 2016.

Obu, J., Westermann, S., Bartsch, A., Berdnikov, N., Christiansen, H. H., Dashtseren, A., Delaloye, R., Elberling, B., Etzelmüller, B., Kholodov, A., Khomutov, A., Kääb, A., Leibman, M. O., Lewkowicz, A. G., Panda, S. K., Romanovsky, V., Way, R. G., Westergaard-Nielsen, A., Wu, T., Yamkhin, J. and Zou, D.: Northern Hemisphere permafrost map based on TTOP modelling for 2000–2016 at 1 km2 scale, Earth-Science Rev., 193(October 2018), 299–316, doi:10.1016/j.earscirev.2019.04.023, 2019.

Orsolini, Y., Wegmann, M., Dutra, E., Liu, B., Balsamo, G., Yang, K., de Rosnay, P., Zhu, C., Wang, W., Senan, R. and Arduini, G.: Evaluation of snow depth and snow cover over the Tibetan Plateau in global reanalyses using in situ and satellite remote sensing observations, Cryosph., 13(8), 2221–2239, doi:10.5194/tc-13-2221-2019, 2019.

Pepin, N., Bradley, R. S., Diaz, H. F., Baraer, M., Caceres, E. B., Forsythe, N., Fowler, H., Greenwood, G., Hashmi, M. Z., Liu, X. D., Miller, J. R., Ning, L., Ohmura, A., Palazzi, E., Rangwala, I., Schöner, W., Severskiy, I., Shahgedanova, M., Wang, M. B., Williamson, S. N. and Yang, D. Q.: Elevation-dependent warming in mountain regions of the world, Nat. Clim. Chang., 5(5), 424–430, doi:10.1038/nclimate2563, 2015.

Pomeroy, J. W., Gray, D. M., Brown, T., Hedstrom, N. R., Quinton, W. L., Granger, R. J. and Carey, S. K.: The cold regions hydrological model: a platform for basing process representation and model structure on physical evidence, Hydrol. Process., 21(19), 2650–2667, doi:10.1002/hyp.6787, 2007.

Qiao, B., Zhu, L. and Yang, R.: Temporal-spatial differences in lake water storage changes and their links to climate change throughout the Tibetan Plateau, Remote Sens. Environ., 222(December 2018), 232–243, doi:10.1016/j.rse.2018.12.037, 2019.

Qin, Y., Yang, D., Gao, B., Wang, T., Chen, J., Chen, Y., Wang, Y. and Zheng, G.: Impacts of climate warming on the frozen ground and eco-hydrology in the Yellow River source region, China, Sci. Total Environ., 605–606, 830–841, doi:10.1016/j.scitotenv.2017.06.188, 2017.

Qin, Y., Chen, J., Yang, D. and Wang, T.: Estimating Seasonally Frozen Ground Depth From Historical Climate Data and Site Measurements Using a Bayesian Model, Water Resour. Res., 54(7), 4361–4375, doi:10.1029/2017WR022185, 2018.

Qin, Y., Wu, T., Zhang, P., Liu, W., Xue, S. and Guo, Z.: Spatiotemporal freeze–thaw variations over the Qinghai-Tibet Plateau 1981–2017 from reanalysis, Int. J. Climatol., 41(2), 1438–1454, doi:10.1002/joc.6849, 2021.

Ran, Y., Li, X. and Cheng, G.: Climate warming over the past half century has led to thermal degradation of permafrost on the Qinghai–Tibet Plateau, Cryosph., 12(2), 595–608, doi:10.5194/tc-12-595-2018, 2018.

Richards, L. A.: CAPILLARY CONDUCTION OF LIQUIDS THROUGH POROUS MEDIUMS, Physics (College. Park. Md)., 1(5), 318–333, doi:10.1063/1.1745010, 1931.

Richardson, L. F.: Weather Prediction by Numerical Process, Cambridge University Press., 1922.

Schaaf, C. and Wang, Z.: MCD43A3 MODIS/Terra+ Aqua BRDF/Albedo Daily L3 Global—500 m V006, NASA EOSDIS L. Process. DAAC, 10, 2015.

Searle, M. P., Parrish, R. R., Hodges, K. V., Hurford, A., Ayres, M. W. and Whitehouse, M. J.: Shisha Pangma Leucogranite, South Tibetan Himalaya: Field Relations, Geochemistry, Age, Origin, and Emplacement, J. Geol., 105(3), 295–318, doi:10.1086/515924, 1997.

Shangguan, W., Dai, Y., Liu, B., Zhu, A., Duan, Q., Wu, L., Ji, D., Ye, A., Yuan, H., Zhang, Q., Chen, D., Chen, M., Chu, J., Dou, Y., Guo, J., Li, H., Li, J., Liang, L., Liang, X., Liu, H., Liu, S., Miao, C. and Zhang, Y.: A China data set of soil properties for land surface modeling, J. Adv. Model. Earth Syst., 5(2), 212–224, doi:10.1002/jame.20026, 2013.

Shangguan, W., Hengl, T., Mendes de Jesus, J., Yuan, H. and Dai, Y.: Mapping the global depth to bedrock for land surface modeling, J. Adv. Model. Earth Syst., 9(1), 65–88, doi:10.1002/2016MS000686, 2017.

Shean, D. E., Bhushan, S., Montesano, P., Rounce, D. R., Arendt, A. and Osmanoglu, B.: A Systematic, Regional Assessment of High Mountain Asia Glacier Mass Balance, Front. Earth Sci., 7(January), 1–19, doi:10.3389/feart.2019.00363, 2020.

Simons, G. W. H., Koster, R. and Droogers, P.: HiHydroSoil v2.0 - A high resolution soil map of global hydraulic properties, Wageningen, The Netherlands. [online] Available from: https://www.futurewater.nl/wp-content/uploads/2020/10/HiHydroSoil-v2.0-High-Resolution-Soil-Maps-of-Global-Hydraulic-Properties.pdf, 2020.

Sjöberg, Y., Jan, A., Painter, S. L., Coon, E. T., Carey, M. P., O'Donnell, J. A. and Koch, J. C.: Permafrost Promotes Shallow Groundwater Flow and Warmer Headwater Streams, Water Resour. Res., 57(2), 1–20, doi:10.1029/2020WR027463, 2021.

Song, L., Wang, L., Li, X., Zhou, J., Luo, D., Jin, H., Qi, J., Zeng, T. and Yin, Y.: Improving Permafrost Physics in a Distributed Cryosphere-Hydrology Model and Its Evaluations at the Upper Yellow River Basin, J. Geophys. Res. Atmos., 125(18), 1–22, doi:10.1029/2020JD032916, 2020.

Vionnet, V., Brun, E., Morin, S., Boone, A., Faroux, S., Le Moigne, P., Martin, E. and Willemet, J.-M.: The detailed snowpack scheme Crocus and its implementation in SURFEX v7.2, Geosci. Model Dev., 5(3), 773–791, doi:10.5194/gmd-5-773-2012, 2012.

Walvoord, M. A. and Kurylyk, B. L.: Hydrologic Impacts of Thawing Permafrost—A Review, Vadose Zo. J., 15(6), 0, doi:10.2136/vzj2016.01.0010, 2016.

Wang, C., Zhao, W. and Cui, Y.: Changes in the Seasonally Frozen Ground Over the Eastern Qinghai-Tibet Plateau in the Past 60 Years Characteristics of Seasonally Frozen, , 8(July), 1–11, doi:10.3389/feart.2020.00270, 2020a.

Wang, G., Li, Y., Hu, H. and Wang, Y.: Synergistic effect of vegetation and air temperature changes on soil water content in alpine frost meadow soil in the permafrost region of Qinghai-Tibet, Hydrol. Process., 22(17), 3310–3320, doi:10.1002/hyp.6913, 2008.

Wang, G., Lin, S., Hu, Z., Lu, Y., Sun, X. and Huang, K.: Improving Actual Evapotranspiration Estimation Integrating Energy Consumption for Ice Phase Change Across the Tibetan Plateau, J. Geophys. Res. Atmos., 125(3), 1–13, doi:10.1029/2019JD031799, 2020b.

Wang, L., Yi, C., Xu, X., Schütt, B., Liu, K. and Zhou, L.: Soil properties in two soil profiles from terraces of the Nam Co Lake in Tibet, China, J. Mt. Sci., 6(4), 354–361, doi:10.1007/s11629-009-1017-3, 2009.

Wang, Q., Fan, X. and Wang, M.: Recent warming amplification over high elevation regions across the globe, Clim. Dyn., 43(1–2), 87–101, doi:10.1007/s00382-013-1889-3, 2014.

Wang, X. and Gao, B.: Frozen soil change and its impact on hydrological processes in the Qinghai Lake Basin, the Qinghai-Tibetan Plateau, China, J. Hydrol. Reg. Stud., 39(January), 100993, doi:10.1016/j.ejrh.2022.100993, 2022.

Wang, Y., Yang, H., Gao, B., Wang, T., Qin, Y. and Yang, D.: Frozen ground degradation may reduce future runoff in the headwaters of an inland river on the northeastern Tibetan Plateau, J. Hydrol., 564(May), 1153–1164, doi:10.1016/j.jhydrol.2018.07.078, 2018.

Westermann, S., Schuler, T. V., Gisnås, K. and Etzelmüller, B.: Transient thermal modeling of permafrost conditions in Southern Norway, Cryosph., 7(2), 719–739, doi:10.5194/tc-7-719-2013, 2013.

Westermann, S., Langer, M., Boike, J., Heikenfeld, M., Peter, M., Etzelmüller, B. and Krinner, G.: Simulating the thermal regime and thaw processes of ice-rich permafrost ground with the land-surface model CryoGrid 3, Geosci. Model Dev., 9(2), 523–546, doi:10.5194/gmd-9-523-2016, 2016.

Westermann, S., Ingeman-Nielsen, T., Scheer, J., Aalstad, K., Aga, J., Chaudhary, N., Etzelmüller, B., Filhol, S., Kääb, A., Renette, C., Schmidt, L. S., Schuler, T. V, Zweigel, R. B., Martin, L., Morard, S., Ben-Asher, M., Angelopoulos, M., Boike, J., Groenke, B., Miesner, F., Nitzbon, J., Overduin, P., Stuenzi, S. M. and Langer, M.: The CryoGrid community model (version 1.0) -- a multi-physics toolbox for climate-driven simulations in the terrestrial cryosphere, Geosci. Model Dev. Discuss., 2022, 1–61, doi:10.5194/gmd-2022-127, 2022.

Wu, Q. and Zhang, T.: Recent permafrost warming on the Qinghai-Tibetan Plateau, J. Geophys. Res., 113(D13), D13108, doi:10.1029/2007JD009539, 2008.

Wünnemann, B., Yan, D. and Ci, R.: Morphodynamics and lake level variations at Paiku Co, southern Tibetan Plateau, China, Geomorphology, 246, 489–501, doi:10.1016/j.geomorph.2015.07.007, 2015.

Yang, K., Wu, H., Qin, J., Lin, C., Tang, W. and Chen, Y.: Recent climate changes over the Tibetan Plateau and their impacts on energy and water cycle: A review, Glob. Planet. Change, 112, 79–91, doi:10.1016/j.gloplacha.2013.12.001, 2014a.

Yang, S., Zhang, H., Kong, M., Liu, Y., Liu, H. and Xu, R.: Study on surficial soil geochemistry in the high-elevation and -frigid mountainous region: A case of Qulong porphyry copper deposit in Tibet, J. Geochemical Explor., 139, 144–151, doi:10.1016/j.gexplo.2013.06.001, 2014b.

Yang, Y., Wu, Q., Jin, H., Wang, Q., Huang, Y., Luo, D., Gao, S. and Jin, X.: Delineating the hydrological processes and hydraulic connectivities under permafrost degradation on Northeastern Qinghai-Tibet Plateau, China, J. Hydrol., 569(November 2018), 359–372, doi:10.1016/j.jhydrol.2018.11.068, 2019.

Yao, F., Wang, J., Yang, K., Wang, C., Walter, B. A. and Crétaux, J.-F.: Lake storage variation on the endorheic Tibetan Plateau and its attribution to climate change since the new millennium, Environ. Res. Lett., 13(6), 064011, doi:10.1088/1748-9326/aab5d3, 2018.

Yi, S., Arain, M. A. and Woo, M.-K.: Modifications of a land surface scheme for improved simulation of ground freeze-thaw in northern environments, Geophys. Res. Lett., 33(13), L13501, doi:10.1029/2006GL026340, 2006.

Yuan, Z., Jin, H., Wang, Q., Wu, Q., Li, G., Jin, X. and Ma, Q.: Profile distributions of soil organic carbon fractions in a permafrost region of the Qinghai–Tibet Plateau, Permafr. Periglac. Process., 31(4), 538–547, doi:10.1002/ppp.2055, 2020.

https://doi.org/10.5194/hess-2022-241
Preprint. Discussion started: 18 July 2022
© Author(s) 2022. CC BY 4.0 License.

Hydrology and Earth System Sciences
Open Access
EGU
Discussions

Zhang, G., Yao, T., Piao, S., Bolch, T., Xie, H., Chen, D., Gao, Y., O'Reilly, C. M., Shum, C. K., Yang, K., Yi, S., Lei, Y., Wang, W., He, Y., Shang, K., Yang, X. and Zhang, H.: Extensive and drastically different alpine lake changes on Asia's high plateaus during the past four decades, Geophys. Res. Lett., 44(1), 252–260, doi:10.1002/2016GL072033, 2017.

Zhang, G., Nan, Z., Wu, X., Ji, H. and Zhao, S.: The Role of Winter Warming in Permafrost Change Over the Qinghai-Tibet Plateau, Geophys. Res. Lett., 46(20), 11261–11269, doi:10.1029/2019GL084292, 2019.

Zhang, G., Yao, T., Xie, H., Yang, K., Zhu, L., Shum, C. K., Bolch, T., Yi, S., Allen, S., Jiang, L., Chen, W. and Ke, C.: Response of Tibetan Plateau lakes to climate change: Trends, patterns, and mechanisms, Earth-Science Rev., 208(July), 103269, doi:10.1016/j.earscirev.2020.103269, 2020.

Zhang, G., Bolch, T., Chen, W. and Crétaux, J.-F.: Comprehensive estimation of lake volume changes on the Tibetan Plateau during 1976–2019 and basin-wide glacier contribution, Sci. Total Environ., 772, 145463, doi:10.1016/j.scitotenv.2021.145463, 2021a.

Zhang, G., Nan, Z., Zhao, L., Liang, Y. and Cheng, G.: Qinghai-Tibet Plateau wetting reduces permafrost thermal responses to climate warming, Earth Planet. Sci. Lett., 562, 116858, doi:10.1016/j.epsl.2021.116858, 2021b.

Zhang, H., Immerzeel, W. W., Zhang, F., de Kok, R. J., Chen, D. and Yan, W.: Snow cover persistence reverses the altitudinal patterns of warming above and below 5000 m on the Tibetan Plateau, Sci. Total Environ., 803, 149889, doi:10.1016/j.scitotenv.2021.149889, 2022.

Zhang, Y., Ohata, T. and Kadota, T.: Land-surface hydrological processes in the permafrost region of the eastern Tibetan Plateau, J. Hydrol., 283(1–4), 41–56, doi:10.1016/S0022-1694(03)00240-3, 2003.

Zou, D., Zhao, L., Sheng, Y., Chen, J., Hu, G., Wu, T., Wu, J., Xie, C., Wu, X., Pang, Q., Wang, W., Du, E., Li, W., Liu, G., Li, J., Qin, Y., Qiao, Y., Wang, Z., Shi, J. and Cheng, G.: A new map of permafrost distribution on the Tibetan Plateau, Cryosph., 11(6), 2527–2542, doi:10.5194/tc-11-2527-2017, 2017.

Zweigel, R. B., Westermann, S., Nitzbon, J., Langer, M., Boike, J., Etzelmüller, B. and Vikhamar Schuler, T.: Simulating Snow Redistribution and its Effect on Ground Surface Temperature at a High-Arctic Site on Svalbard, J. Geophys. Res. Earth Surf., 126(3), 1–21, doi:10.1029/2020JF005673, 2021.